University of Benghazi
Faculty of Information Technology
Department of Computer Science

Automated Glaucoma Detection based on Combination of Feature Extraction Methods

By
Zakia Ahmed Ali

Supervisor
Ahmed Lawgali
Associate Professor
Co-Supervisor
Mohamed Abdalla
Assistant Professor

Thesis was Submitted in Partial Fulfillment of The Requirements for The Degree of Master in Computer Science.

Date 25/1//2023

University of Benghazi **Faculty of Information Technology**

Department of Computer Science

Automated Glaucoma Detection based on Combination of Feature Extraction Methods

By

Zakia Ahmed Ali

This Thesis was Successfully Defended and Approved on: . .2023

Supervisor

Ahmed Lawgali

Signature: .....

Co-Supervisor

Mohamed Abdalla

Signature: .....

Dr. Salwa Elakeili **(Internal examiner)**

Signature: .....

Dr. Almabruk Sultan **(External examiner)**

Signature: .....

(Dean of Faculty) **(Director of Graduate studies and training)**

Dr.Abdelsalam Maatuk **Dr otman mohammed Albadri**

Dedication

To my parents and my near soul Mahmoud, this thesis is dedicated to their love and endless support.

Zakia Ahmed

Publications

ICEEIT 2022: (Published)

Z. Ahmed, A. Lawgali and M. Abdalla, "Automated Glaucoma Detection based on LBP Representation and GLRLM Feature Extraction Method," *2022 International Conference on Engineering & MIS (ICEMIS)*, 2022, pp. 1-6, doi: 10.1109/ICEMIS56295.2022.9914267.

Acknowledgments

Primarily I would like to thank Allah for every blessing that gives me the ability to success and complete this thesis.

Secondly, I would thank my teacher and guide Dr. Ahmed Lawgali for his faithful teaching, guidelines and his support that helps me to patch this project.

I also like to extent my gratitude to Dr. Mohamed Abdalla for his guidelines and endless encouragement.

Then I would to express special thanks to Ophthalmology Experts for their cooperation and give me their knowledge:

Dr. Ahmed Janjan

Dr. Chiraz Boujemaa

Dr. Mahmoud Ahmed Arnaouty

Dr. Masoud Alawamy

Prof. Sabah Eldressi

Dr. Sadina Bader Mohamed

TABLE OF CONTENTS

LIST OF TABLES

LIST OF FIGURES

LIST OF OBSERVATIONS

Observation	Meaning
2D-DWT	2D-Discrete Wavelet Transform
2D-FBSE-EWT	Two Dimensional Fourier-Bessel Series Expansion based Empirical Wavelet Transform
3DCNN	Three-Dimensional Convolutional Neural Network
ANFIS	Adptive Neuro-Fuzzy Inference System
CAD	Computer Aided Diagnosis
CDR	Cup to Disc Ratio
CLAHE	Contrast-Limited Adaptive Histogram Equalization
CTREE	Conditional Inference TREE
CNN	Convolutional Neural Network
DCGAN	Deep Convolutional Generative Adversarial Network
EWT	Empirical Wavelet Transform
FOS	First Order Statistical
GAN	Generative Adversarial Network
GLCM	Gray Level Co-occurrence Matrix
GLRLM	Gray Level Run-Length Matrix
HCSC	Hospital Clinico Universitario San Carlos
HE	Histogram Equalization
HOC	Higher Order Cumulant
HOG	Histogram of Oriented Gradient
HOS	Higher Order Spectra
HUC	Hospital Universitario de Canarias
HUMS	Hospital Universitario Miquel Servet
IDWT	Inverse Discrete Wavelet Transform
ISNT	Inferior, Superior, Nasal and Temporal
KNN	K-Nearest Neighbor
LARKIFCM	Level set based Adaptively Regularized Kernel based Intuitionistic Fuzzy C Means
LBP	Local Binary Pattern

LDA	Linear Discriminant Analysis
LR	Logistic Regression
LS-SVM	Least Square- Support Vector Machine
MLP	Multi-Layer Perceptron
NB	Naive Bayes
NN	Neural Network
OCT	Optical Coherence Tomography
PCA	Principle Component Analysis
RIM-ONE	Retinal IMage database for Optic Nerve Evaluation
RF	Random Forest
ROI	Region Of Interest
SDOCT	Spectral Domain Optical Coherence Tomography
SFFS	Sequential Floating Forward Selection
SOM	Self-Organized Map
SMO	Sequential Minimal Optimization
SVM	Support Vector Machine
WHO	World Health Organization

Automated Glaucoma Detection based on Combination of Feature Extraction Methods

By

Zakia Ahmed Ali

Supervisor

Dr. Ahmed Lawgali

Co- Supervisor

Dr. Mohamed Abdalla

Abstract

Machine learning techniques have been using increasingly in medical image analysis field to perform features recognition and decision-making tasks that demonstrate major advances in medical care field. Automated analysis of medical images contributes to increase the classification performance. Increasing the number of glaucoma patients in our country motivated us to establish an automated system for detecting the disease. Glaucoma is chronic and degenerative disease causing irreversible damage in nerve system of an eye and is led to blindness. This research aimed to present an automated glaucoma detection approach by identifying non-morphological attributes using combination of feature extraction methods. The proposed methodology was divided into: image acquisition through RIM-ONEs datasets, 2D-Discrete Wavelet Transform was applied to de-noising databases images. Local Binary Pattern represented the separated images and Gray Level Run-Length Matrix used to describe the texture patterns. Finally, two classifiers were applied to learn the models using extracted features, the proposed methodology was evaluate by measuring the sensitivity, specificity and accuracy of the models and the results were promising and more accurate compared to the results of related literatures.

Keywords: Glaucoma, Local Binary Pattern, Gray Level Run-Length Matrix.

CHAPTER ONE

Introduction

1.1 Overview

From 1980s, Machine Learning as a field of Artificial Intelligence is used to learn a pattern from data without programming (Mayro, Wang, Elze, & Pasquale, 2020). Machine learning schema made up of several processes such as image preprocessing, image segmentation, feature extraction and classification. The machine learning classifier algorithms work in two phases, first phase is training where algorithms used the extracted features of data (images) to construct the model, the second phase is testing the model to check its accuracy depending on the output of learned model (Rajyaguru, Vithalani, & Thanki, 2020). Essential phase is training step using iterative process which the algorithm learns pattern from data to make prediction and classification (Medeiros, Jammal, & Thompson, 2019).

In a short time, machine learning algorithms were involved in many disciplines as healthcare, ophthalmology, etc. In ophthalmology, machine learning algorithms applied to detect many eye diseases such as diabetic retinopathy (Romany F Mansour, 2017), cataract (Xu, Zhang, Li, Guan, & Zhang, 2019), age-macular degeneration (Burlina et al., 2017) and glaucoma (Goldbaum et al., 1994).

In 2020, 76 million person were affected from glaucoma with global prevalence of 3.5% (Mayro et al., 2020), and it will increasing to 111.8 million in 2040 (Gómez-Valverde et al., 2019). Glaucoma is one of the most popular eye disease in the green mountain area in Libya, where the percentage of glaucoma patients was rapidly increasing that led us to study this phenomenon.

According to World Health Organization (WHO), glaucoma is the second largest causes of blindness in the world (Bisneto, de Carvalho Filho, & Magalhães, 2020) (Kumar, Seelamantula, Kamath, & Jampala, 2019). In early stages, glaucoma symptoms are not appeared as visual field affected to loss 20 – 50% of retinal ganglion cells (Mayro et al., 2020). Only 10 – 50 % of glaucoma patients aware that they suffer from that diseases (Gómez-Valverde et al., 2019).

Essential effects of glaucoma are an optic nerve damage and loss of retinal nerve fiber layer its characteristics due to elevation of intraocular pressure inside the eye (Kumar et al., 2019) (Serener & Serte, 2019).

Various methods were used to glaucoma diagnosis that involved intraocular pressure measurement, visual field testing and retinal images (Septiarini & Harjoko, 2015). Indicate glaucoma using intraocular pressure only is not effective, because some glaucoma patients have normal eye pressure, visual field test is expensive and not available in many clinics, the previous tests were performed by experts which the diagnosis accuracy affected to the limitation of experts domain knowledge (Septiarini & Harjoko, 2015). The most appropriate method and widely used in glaucoma screening was retinal images (Orlando et al., 2020) (Serener & Serte, 2019). Availability of fundus images as in Figure 1.1 in primary care and its popularity in eye diseases explain why this imaging modality was interest in many researches (Medeiros et al., 2019) (Gómez-Valverde et al., 2019).

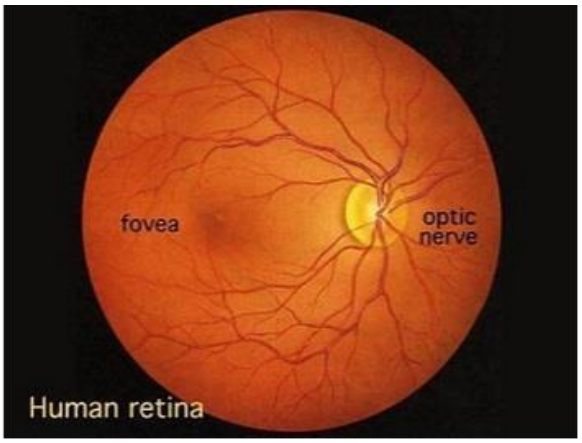

Figure 1.1: Standard Fundus image of the eye.

The occurred damage changes the structure of retina, the retinal images observe the structure of retina as fundus images (Septiarini & Harjoko, 2015). Features that extracted from fundus images were analyzed and used to discriminate between glaucoma and healthy classes, where they described each interest region in image (Bisneto et al., 2020).

Machine learning techniques have been applied in glaucoma detection problem, where many algorithms used to localize or segment images (Sevastopolsky et al., 2019), and numerous of them employed the data to extract the features (Kavya & Padmaja, 2017) (Septiarini & Harjoko, 2015) that identified relevant information that presented in medical images. Classification using machine learning algorithms was applied to detect glaucoma and healthy image in (Diaz-Pinto et al., 2019) (Saba, Bokhari, Sharif, Yasmin, & Raza, 2018) (Cerentini, Welfer, d'Ornellas, Haygert, & Dotto, 2018).

In glaucoma detection, researches that used non-morphological features had accuracy higher than that used morphological features (Septiarini & Harjoko, 2015). Non-morphological features involve texture analysis, transform analysis and spatial analysis (Krishnamoorthi & Chinnababu, 2019), which provide physical properties information such as appearance, intensity, structural changes, etc.

1.2 Research Motivation

Our country testify increasing the spread of specific human diseases as Vitamin D Deficiency, Gastric cancer, Tuberculosis, Lymphoma and Glaucoma. Each disease needs to research the causes and early identification. Artificial intelligence and machine learning had important and efficient effect in medical diagnosis (Computer Aided Diagnosis (CAD)), with the using of machine learning techniques to early glaucoma detection can prevent patients vision and keep life quality.

Many techniques were performed in glaucoma detection. This work was developed model that used feature extraction methods to identify efficient features that classified retinal fundus images and achieved high performance to validate the glaucoma detection model.

1.3 Problem Statement

Glaucoma is serious illness that causes blindness and effected on millions of people around the world. Early detection of glaucoma is necessary to prevent vision loss, where detection the disease in early stages is difficult task for ophthalmology experts, usually they detected the glaucoma in moderate stage. In addition, many measurements were applied to detect glaucoma such as visual field test, intraocular pressure measurements and medical imaging that means manually diagnosis of glaucoma is time consuming and expensive (Wu et al., 2022). Many automated methodologies proposed to detect glaucoma disease with different ratio of performance. The main challenge is obtaining high performance in glaucoma detection using reliable data without sophisticated methods as deep learning that time consuming and need robust resources.

To overcome that challenges of need specific expertise and long time of manual practice, and to improve the performance and accuracy of classifier model, an automated detection of glaucoma using machine learning techniques was proposed based on medical images.

1.4 Research Aims and Objectives

This work aimed to present methodology for CAD system to detect glaucoma disease from fundus images by applying techniques to extract the feature in a manner that obtained distinguish non-morphological features to obtain high performance.

Objectives to achieve that aim as followed:

- To review and understand glaucoma conditions, many studies were reviewed.
- To preprocess the obtained images, 2-Dimentional Discrete Wavelet Transform (2D-DWT) was applied.
- To extract non-morphological features, Local Binary Pattern (LBP) and Gray Level Run-Length Matrix (GLRLM) methods were performed.
- To obtain all benefits of extracted features, the extracted features were reduced using Linear Discriminant Analysis (LDA) technique.
- To produce trained model, Support Vector Machine (SVM) and Random Forest (RF) classifiers were implemented.
- Evaluate the learned models, perform comparison between their accuracies using testing set and calculate accuracy, sensitivity and specificity for each model and comparing our results with reviewed studies.

1.5 Research Methodology

The main idea of our work was classify retinal images (fundus images) to normal and glaucoma images based on extracted features.

1.5.1 Literature Review:

Many glaucoma detection researches were studied to obtain information about glaucoma, the challenges and how to detect. Most sources of these studies were published in Elsevier, IEEE and Spring. The proposed database was RIM-ONE version 1, 2 and 3 that used in our research had reliable images resource from three hospitals in Spain and each image was classified by five ophthalmology experts.

1.5.2 Problem Definition and Analysis:

This work needs to use just one of the measurements (medical image) that used to detect glaucoma disease by experts that means the quality of the images and the severity degree of disease played critical role in the detection of glaucoma.

1.5.3 Research Design:

The research was designed as followed steps:

- Review the related studies of automated glaucoma detection.
- Define glaucoma detection problem, its challenges and CAD stages.
- Propose techniques to solve a problem and implement different experiments.
- Analyze the results and evaluate misclassified images using ophthalmology experts.
- Compare the obtained results of the proposed experiments, and compare the best experiment results with reviewed previous studies.

1.6 Scope of Research

There were many models that developed to glaucoma detection that models presented different phases of model construct as preprocessing, segmentation, feature extraction and classification. Our work focused on extracted the features form fundus images using LBP and GLRLM methods that contributed to identify glaucoma. The used datasets (RIM-ONE version 1, 2 and 3) consist of Region Of Interest (ROI) in fundus images which led us to focus on image preprocessing, feature extraction and classification stages.

1.7 Thesis Organization

- Chapter 2 overviewed the role of machine learning in medical image diagnosis, glaucoma disease, the detection problem and CAD stages that consisted of : image preprocessing, feature extraction, dimensionality reduction and classification.
- Chapter 3 reviewed the previous related researches of our topic, presented their techniques, performance and how to converge with our work.
- Chapter 4 explained the proposed methodology with description of the used databases. The used techniques also proposed in this chapter with their advantages.
- Chapter 5 represented the experiments that performed in this research and their results, evaluated misclassified data by experts and presented the comparison with reviewed previous researches.
- Chapter 6 involved the conclusion, research limitations and future work to improve the glaucoma detection performance.

CHAPTER TWO

Background

The previous section discussed the overview of research problem, our motivation, aim and how to reach to that aim. This section presented an overview of glaucoma disease, anatomy of an eye, the reason of glaucoma, the challenges that stand up of glaucoma detection and how to be detected using CAD systems.

2.1 Glaucoma

Glaucoma, silent thief of sight, is an asymptomatic disease affect due to increase intra-ocular pressure in retina and leads to structure and functional changes (Shinde, 2021). Structural changes involve change in optic nerve head structure, decrease in neuroretinal rim area and damage in retinal nerve fiber layer (Kavya & Padmaja, 2017). Functional change as vision lost possibly occurred before significant loss of nerve fibers (Kavya & Padmaja, 2017). Seriousness in glaucoma disease involves just 10 – 50% of patients are aware of disease progression before advanced stage occurs when their visions are irreversibly lost (Orlando et al., 2020) (Weinreb, Aung, & Medeiros, 2014). The effect of glaucoma disease on the vision was demonstrated in Figure 2.1.

Figure 2.1: The vision loss effect of Glaucoma Disease.

Globally, the statistics indicated an increase in infection rates especially people that their ages between 40-60 with ratio 3 - 4% of them (Tham et al., 2014). In 2013, the number of person around the world that suffered from glaucoma reached to 65 million and reached to 80 million in 2020 as the WHO announced (Claro et al., 2019), by 2040

will be 111.8 million and 10% of patient will become blindness (dos Santos Ferreira, de Carvalho Filho, de Sousa, Silva, & Gattass, 2018). Glaucoma Research Foundation reported in 2017 that glaucoma was the second cause for blindness in the world after cataracts disease (dos Santos Ferreira et al., 2018). Although the surgery can be reversibly the vision in cataracts disease, but blindness in glaucoma is permanent (Shinde, 2021) (de Sousa et al., 2017) (Bisneto et al., 2020). Early detection of glaucoma is critical to decrease or stop disease progressing.

Imaging techniques that used to glaucoma detection listed as fundus images, Optical Coherence Tomography (OCT), scanning laser polarimetry and Heidelberg retina tomography. Recently, scanning laser polarimetry and confocal scanning laser ophthalmoscopy methods were not used for clinical diagnosis of diseases (Zheng, Johnson, Garg, & Boland, 2019).

The availability of fundus photograph and its low cost compared to other retinal image modalities made them the best tool for many ophthalmic diseases as diabetic retinopathy, age-related macular degeneration and glaucoma (Orlando et al., 2020).

Recent study (Mayro et al., 2020) showed that many experts agreement on diagnosis the damage of optic nerve head only in moderate stage of disease from fundus images, that difficulty of detection caused due to compound by variation of image capture platforms, focus, magnification and had non-glaucoma disease. Fundus image could not easily recognize glaucoma in early stages, usually fundus image was complementary with other assessment as intraocular pressure measurement, OCT, standard automated perimetry to assess visual field (Orlando et al., 2020).

2.2 Eye Anatomy

The part that transmits the images from eye to brain is the optic nerve. The optic nerve is the collection of millions of nerve fibers (axons) of the eye retina, where the optic disc is the cross sectional view of it (Kumar et al., 2019). Optic disc is the region where blood vessels and nerve fibers enter the retina, the central bright area of the optic disc is the optic cup that lies within the optic disc, and the peripheral region between optic disc and optic cup called neuroretinal rim (Bajwa et al., 2019) as showed in Figure 2.2.

Eye fluid termed as "aqueous humor" secretes inside the eye, it produces and flows regularly through the channel, which resulting stable in intraocular pressure (Kavya & Padmaja, 2017). Due to abnormal drain or production in the aqueous humor circulating

inside the eye between the lens and cornea that causes intraocular fluid pressure (Kumar et al., 2019). The increasing in intraocular pressure causes changing the structure of an eye anatomy where it causes damage in retinal nerve fibers that constituting optic nerve and changes the characteristics of optic disc such as enlarges the optic cup size termed as Cupping phenomenon and changes the color of optic disc from pink to pale (M.-L. Huang, Chen, & Huang, 2007). (Jackson & Radhakrishnan, 2014) reported the

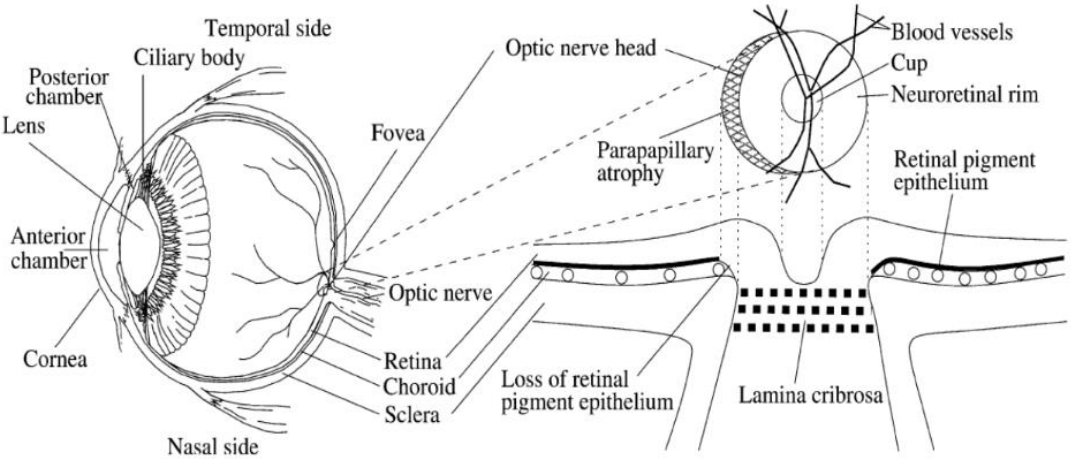

Figure 2.2: The Terminologies of the Eye and the Optic Nerve Head Structure.

damage in optic nerve fibers was observed when about 40% of axons losted. The loosed axons causes to reduce the functional capability of the retina and the visual information may can not transmitted to the brain, which leads to visual field loss then to blindness (Simón, Alonso, & Antón, 2005).

The meaningful parameter for glaucoma detection ophthalmologists relied on is Cup-to-Disc Ratio (CDR) that proposed by Kumar *et al*. (Kumar et al., 2019), where cup diameter and disc diameter used to obtain CDR. In 90% of normal eyes, the value of CDR is 0.1 to 0.3, where in glaucoma eye the CDR value between 0.5 and 0.7 in moderate glaucoma eye, for serve cases is more than 0.7 (Septiarini & Harjoko, 2015) (Shinde, 2021). Other structure indicator of glaucoma is the values of Inferior, Superior, Nasal and Temporal (ISNT) parts that obtained from rim area, which divides to four parts (Septiarini & Harjoko, 2015).

Although, the cause of blockage is unknown, but it tends to the effect of other diseases as diabetes, steroids medication, ethnicity and to the old age (Jackson &

Radhakrishnan, 2014). WHO reported (Sevastopolsky et al., 2019) that the people in poor income countries and industrialized regions were susceptible to eye related diseases compared with other regions.

Although, that chronic disease can not be revive loosed axons. Some suggested life-long treatment found such as eye drops that controlled the intraocular pressure, laser procedure and in advanced stages microscopic surgeries performed to decrease the intraocular pressure by increasing the drainage (Orlando et al., 2020). Early diagnosis essential to prevent the vision and increase life quality.

2.3 Glaucoma Detection

Traditional methods to diagnosis glaucoma by ophthalmologists included intraocular pressure, visual field loss test and medical history that evaluated by ophthalmoscopy (Quigley & Broman, 2006). However, these evaluations need time and required human interaction and may have subjective errors.

To overcome these challenges, many studies were worked on medical imaging analysis field using machine learning techniques for glaucoma detection. The biomedical image had been progressed and advanced in disease diagnosis, where detection the glaucoma using retinal images was one of the active medical area in research (Chaudhary & Pachori, 2021). Using techniques of digital processing of biomedical image given support for diagnosis, which improved appearance of texture features and provided more information for decision-making support.

Fundus photograph used to describe interior surface of an eye. ‘‘Fundus’’ is a Latin word, that means the opposite region of a pupile in the eye (Simón et al., 2005). Figure 2.3 presented a comparison between healthy and glaucoma fundus images and the cropped images around optic nerve head that observed the difference among images where the features were extracted. Two types of features were extracted from retinal fundus photograph to detect glaucoma that observed glaucoma eyes where structured features termed as Morphological features and Non-Morphological features (Kavya & Padmaja, 2017). Structure features described the symptoms of disease such as CDR, ISNT and rim area. Texture features are the texture changes in retinal image that occur causing of the symptoms of glaucoma such as color, shape, texture changes in an optic nerve anatomy (Septiarini & Harjoko, 2015).

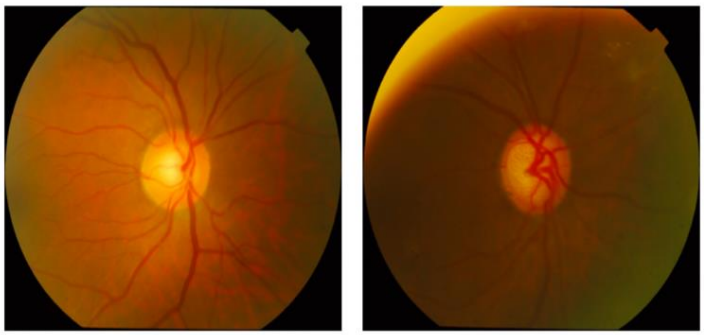

Healthy Fundus Photograph Glaucoma Fundus Photograph

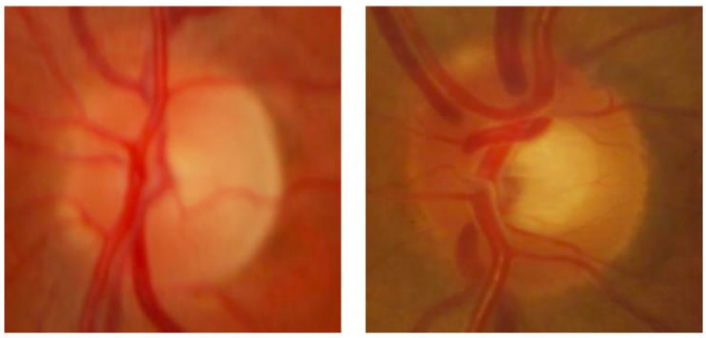

Healthy Fundus Photograph Glaucoma Fundus Photograph

Figure 2.3: Comparison the difference between Glaucoma and Healthy Fundus images.

(Healthy Fundus image in Upper Left, Glaucoma Fundus image in Upper Right, the Lower Fundus images were cropped to ROI around Optic Nerve Head, Healthy image in Lower Left and Glaucoma image in Lower Right).

2.4 Automated Glaucoma Detection

Artificial intelligence created automated systems that perform tasks that require human intelligence as feature recognition and decision-making, etc (Zheng et al., 2019). The goal of learning pattern without explicitly programming the algorithm just from data was achieved in machine learning techniques, which the computing system improved through experiences and input data. Significant promise was coming with machine learning techniques in what algorithms can contribute in disease detection and decision-making (Mayro et al., 2020). Especially the possibility of slowing down the disease was very high if it was diagnosed sufficiently early (Bajwa et al., 2019).

In recent years, machine learning algorithms increasingly had been used to glaucoma detection problem, where the techniques that applied on optical imaging noted the changes and improved detection accuracy compared to human observations (Bowd &

Goldbaum, 2008). The feature extraction methods have ability to describe imperceptible changes in contrast that specialists can not notified, they termed as texture features. Where the texture attributes explore the properties of pixels with their neighbors.

2.5 Challenges of Glaucoma Detection

There were some challenges that hindered automated glaucoma detection, the main challenges were listed as followed:

2.5.1 Large Scale Database

The absence of large number of images in glaucoma databases that available publically had hampered the performance of automated learned algorithms to rapid development as deep learning techniques (Orlando et al., 2020).

2.5.2 Missed Early Diagnosis

In recent study, various experts failed to detect early stage of glaucoma, few images of early glaucoma stage in databases due to 50 – 90% of glaucoma patients were remain undiagnosed (Gómez-Valverde et al., 2019) (dos Santos Ferreira et al., 2018).

2.5.3 Segment Optic Disc and Optic Cup

Delineation the optic cup from optic disc accurately in fundus images was difficult due to the lack of detailed information in fundus photographs and high intensity of blood vessels in optic nerve head region. Haleem *et al.* (Haleem, Han, Van Hemert, & Li, 2013) stated that segment optic disc and optic cup was a difficult process due to invisible line between optic disc and optic cup visually due to pathological changes.

2.5.4 Fundus Image Databases

Many public databases constructed of internet retinal images that evaluated based on their visual appearance without any clinical information as in DRISHTI_GS database, where it labeled based on image characteristics. In addition, in many existed glaucoma databases did not mention any information about the source of clinical diagnosis such as DRIONS and ORIGA databases (Orlando et al., 2020).

Fundus image modality required years of practice and specific expertise to perform subjective interpretation task to identify glaucoma signs.

2.5.5 Several Examination to Detect Glaucoma

Combination of functional and structural testing were consisting the detection of glaucoma such as standard automated perimetry measurement, intraocular pressure, CDR, ISNT and retinal medical image (Septiarini & Harjoko, 2015).

2.6 Phases of CAD System

CAD system is an auxiliary scientific tool to process vast amount of data in short time. CAD system aimed to solve complex clinical problems and increases the medical diagnosis accuracy by providing a second opinion to specialists based on additional information in fast and more accurate detection (dos Santos Ferreira et al., 2018). Medical knowledge and computational algorithms were merged in CAD system (Zhao, Chen, Chen, & Li, 2022). CAD system involved machine learning techniques and consists of: image acquisition, pre-processing, segmentation, feature extraction, feature reduction and classification. Features extraction and classification phases are essential in CAD systems on various computational systems (de Sales Carvalho, Rodrigues, de Carvalho Filho, & Mathew, 2021).

2.6.1 Image Acquisition

One of the most reliable and used database for segmentation and classification glaucoma images purpose was RIMONE database. It is a public database that had healthy and glaucoma fundus images in the three versions of database. The database images were created by three collaborating hospitals that were Hospital Universitario de Canarias (HUC) in Tenerife, Hospital Clinico Universitario San Carlos (HCSC) in Madrid and Hospital Universitario Miquel Servet (HUMS) in Zaragoza, in Spain, and all the images were cropped around ROI and the assessment of database images were performed by specialists in ophthalmologists (Fumero, Alayón, Sanchez, Sigut, & Gonzalez-Hernandez, 2011).

The database repository was accessible through the website of http://medimrg.webs.ull.es.

2.6.2 Pre-processing

In CAD system, preprocessing is one of the critical and important stages, where enhancement and standardization the input images were priority before feature extraction, to improve the fundus image quality and reduce noise and artifacts (de Sales Carvalho et al., 2021). Obtaining clear image from noised image was challenging task.

If the preprocess stage was not performed, that caused decrease in classifiers performance.

2.6.3 Segmentation

Where image was divided to multi-parts to detect region of interest. The successful in segmentation phase determined the successful in image analysis. Segmentation step is an important when morphological structures were extracted, that means this work had not to use segmentation techniques due to non-morphological features were extracted from whole image.

2.6.4 Feature Extraction

It converted the input image to a set of features, where the features used to recognize a pattern and employed to make accurate decisions during classification. Structural and Non-structural features described the internal texture of fundus image. Structural features as CDR, ISNT, and vessels ratio, Non-structural features such as the changes of color, depth and shape of optic disc (Kavya & Padmaja, 2017). This work proposed an automated analysis of medical retinal images to obtain non-structural attributes using texture features extraction methods.

2.6.5 Feature Reduction

Feature reduction techniques selected the most significant parameters that will be useful in discriminated between classes and increased the classifiers performance (An et al., 2018).

2.6.6 Classification

Classification is determined if the image was healthy or glaucoma by model that trained using extracted features of the prior stage. The performance of classifier was evaluated using metrics such as accuracy, sensitivity, specificity, etc. Cross-validation was adapted in CAD system in training the classifier to overcome the issue of overfitting. This work aimed to achieve high results by define features vector that distinguished between pathological and healthy image.

2.7 Summary

Glaucoma is a chronic and degenerative eye disease that causes permanent blindness. It changes the eye structure due to the increase in intraocular pressure. CDR is the most used measurement to screening the glaucoma. To improve the performance of the

detection using traditional methods, many CAD systems were adopted to automated screening of glaucoma using the stages of CAD.

CHAPTER THREE

Literature Review

The previous section presented the concept of glaucoma disease, its reason and the stages of CAD to detect the disease. Many CAD glaucoma systems were presented and how each one contributed in glaucoma detection domain using different features and data. Current section presented those systems and their differences.

Many researches interested with automated glaucoma detection problem, the researchers discussed the detection problem from different aspects, such as the type of used data that adopted to train the model, types of extracted features and the phases that research focused on such as segmentation, feature extraction and classification. An overview of those aspects was presented and discussed their performance as followed:

3.1 Types of Data in Automated Glaucoma Detection

In automated diagnosis of glaucoma, different data types were adopted to detect the disease, the data was the measurement that used to screening the glaucoma using ophthalmologists as visual field data and different retinal images techniques.

3.1.1 Visual Field Data:

When the researcher reviewed the types of data that demonstrated in automated glaucoma diagnosis, visual field data records through standard automated perimetry measurement was one of the data type that used as input data to the first research that proposed in automated detection of glaucoma using machine learning algorithms that introduced by Goldbaum *et al.* (Goldbaum et al., 1994). The performance of two-layered Neural Network (NN) was compared with two experts, the authors investigated that human experts were accurate as the NN learning model in glaucoma detection. The agreement in diagnosis between two experts was 75%, while the agreement between the first expert and the model was 74% and with the second expert was 72%. While no significant disagreement between the two experts and the learned model.

Simon *et al.* (Simón et al., 2005) used visual field assessment using hybrid classifiers of Self-Organized Map (SOM) based classifier and rule-based expert system to detect open angle glaucoma. Eight-layered Convolutional Neural Network (CNN) was trained using visual field of standard automated perimetry measurement to automated

detect glaucoma in (Kucur, Hollo, & Sznitman, 2018). Yousefi, Elze, Pasquale and Boland (Yousefi, Elze, Pasquale, & Boland, 2018) adopted Principle Component Analysis (PCA) to reduce the visual field data space then applied Density-based unsupervised clustering to detect glaucoma, the purpose and techniques of the studies that used visual field data to train their models were listed in Table 3.1.

Table 3.1: Some of automated glaucoma detection studies that used Visual Field data.

Author	Size of Data	Technique	Purpose
(Goldbaum et al., 1994)	120 records of Glaucoma Center at UCSD.	NN	Classify glaucoma and healthy patients.
(Kucur et al., 2018)	465 visual field data from Glaucoma Center of Semmelweis University, Budapest - Hungary.	CNN	Automated detection of glaucoma
(Yousefi et al., 2018)	31591 visual field record from Humphrey Field Analyzers at the Massachusetts Eye and Ear Infirmary.	PCA, manifold learning and density based clustering	Monitoring the stages of glaucoma.
(Simón et al., 2005)	180 visual field clinical records of Glaucoma Unit of the University Hospital of Valladolid - Spain.	Comprising of SOM and rule based expert system	Support the early detection of open angle glaucoma.

Visual field can effected by several eye disease such as myopia, diabetic retinopathy, and cataract diseases, etc. Where it used as a supplement measure to detect glaucoma with intraocular pressure measures, retinal medical images and retinal nerve fiber layer thickness measures.

In addition, the using of data with different resources and the lack of accreditation on available public database of visual field data that helped the researchers to compare their methodologies though it where most of exist studies used standard automated perimetry measurement that collected from hospitals.

3.1.2 Retinal Medical Images:

Other approaches used retinal imaging modalities and restricted on optic nerve head area that was the most affected area in glaucoma detection. The most of reviewed studies were applied the learned approaches using Optical Coherent Tomography (OCT) images and fundus photographs.

OCT is powerful tool to describe quantitatively and qualitatively of glaucoma that provides cross sectional of tissues in retinal images, OCT images describe critical parameters such as retinal nerve fiber layer thickness, depth of optic disc and inner anatomy of an eye layers, that given more accurate results compared to confocal scanning laser ophthalmoscopy (Toshev, Lamparter, Pfeiffer, & Hoffmann, 2017) (An et al., 2019).

Cerentini *et al*. (Cerentini et al., 2018) used OCT to detect glaucoma using genetic algorithm with laser speckle flowgraphy images. In addition, retinal nerve fiber layer thickness was used as a parameter to identify glaucoma that obtained from OCT images as in (M.-L. Huang et al., 2007) that used OCT to detect glaucoma by Adptive Neuro-Fuzzy Inference System. Spectral Domain OCT (SDOCT) were adopted to train ResNet34 deep learning algorithm in (Medeiros et al., 2019) used 32820 pairs of optic disc photographs and retinal nerve fiber layer.

SDOCT with retinal nerve fiber layer thickness had high reproducibility to detect glaucoma accurately. Kim, Cho and Oh (Kim, Cho, & Oh, 2017) used OCT to obtain retinal nerve fiber layer thickness, visual field data and general examination of ophthalmic to detect glaucoma, few of studies that used OCT images in automated glaucoma detection were observed in Table 3.2.

Table 3.2: Some of automated glaucoma detection studies that used OCT images.

Author	Size of Data	Technique	Purpose
(Cerentini et al., 2018)	787 OCT images of Four databases.	GoogLeNet NN	Classify glaucoma images.
(M.-L. Huang et al., 2007)	341 OCT images of participants of Department of Ophthalmology, China Medical University Hospital, Taiwan – China.	Adaptive neuro-fuzzy inference system	Automated classification of glaucoma images.
(Medeiros et al., 2019)	32820 SDOCT images collected from the Duke Glaucoma Repository.	Residual Deep NN	Detect the stages of glaucoma severity.
(Kim et al., 2017)	499 OCT images, visual field data and general ophthalmic examination	C5.0, SVM, RF, K-Nearest Neighbor (KNN)	Automated detection of glaucoma disease.

However, retinal nerve fiber layer thickness reduced also causing of myopia disease not just effected by glaucoma. Although, OCT provides more information as depth, thickness map of retinal nerve fiber layer and detect the boundary of between optic disc and optic cup, but most researchers used fundus images in their studies due to its availability in hospitals.

Instead of OCT images, retinal fundus images were more common in used in glaucoma screening due to its availability and low cost. Table 3.3 presented comparison between public databases of color fundus images in a manner of number of images, the resource of image diagnosis if it was clinical by experts or from internet images and if it prepared for glaucoma classification or for other purpose.

Table 3.3: Comparison between popular public fundus images databases.

Database Name	Num. of Glaucoma	Num. of Normal	Total num. of Images	Diagnosis Resource	Glaucoma Classification
DRIONS (Carmona, Rincón, García-Feijoó, & Martínez-de-la-Casa, 2008)	-	-	110	Not applicable	No
DRISHTI_GS (Sivaswamy, Krishnadas, Joshi, Jain, & Tabish, 2014)	70	31	101	From image	Yes
DR HAGIS (Holm, Russell, Nourrit, & McLoughlin, 2017)	10	29	39	Clinical	Yes
HRF (Odstrcilik et al., 2013)	15	30	45	Clinical	Yes
LES-AV (Odstrcilik et al., 2013)	11	11	22	Clinical	Yes
ORIGA (Zhang et al., 2010)	168	482	650	Not mentioned	Yes
RIGA (Almazroa et al., 2018)	-	-	750	Not mentioned	No
RIM-ONE v1 (Fumero et al., 2011)	51	118	169	Clinical	yes
RIM-ONE v2 (Fumero et al., 2011)	200	255	455	Clinical	yes
RIM-ONE v3 (Fumero et al., 2011)	74	85	159	Clinical	yes

3.2 Types of Features in Automated Glaucoma Detection

Automated glaucoma classification researches used medical retinal images that influenced by features types. The extracted features were divided to morphological (structured) features and non-morphological (non-structured) features.

3.2.1 Morphological (Structural) Features:

Morphological features described the changes in the structure of ROI as in CDR, periapapillary atrophy and RIM area that need to perform segmentation to localize the ROI and determine the structure of features. Nayak, Acharya, Bhat, Shetty and Lim (Nayak, Acharya U, Bhat, Shetty, & Lim, 2009) used morphological features with CNN to glaucoma screening, Chrastek *et al.* (Chrástek et al., 2005) used different features to identify glaucoma as CDR, RIM area and periapapillary atrophy. Shinde (Shinde, 2021) extracted structural features to detect glaucoma from 666 fundus images. ROI was extracted using brightest spot algorithm, next fully CNN was used for optic disc and optic cup segmentation to calculate CDR, ISNT and blood vessel ratio as features of structural changes on optic nerve occurred. The classification was performed by SVM, adaboost and NN.

Most researches used structural features in automated glaucoma detection that restricted the ability to learn more features of other region (Orlando et al., 2020).

3.2.2 Non-Morphological (Non-Structural) Features

Non-morphological features were not had to perform segmentation, where the features were extracted from whole image that derived from color, position and related of pixels as texture and shape. Non-morphological provided smoothness, roughness information and surface reflectance difference (Krishnamoorthi & Chinnababu, 2019), where texture and intensity were different from healthy and glaucoma images due to glaucoma symptoms change the texture of image (Kavya & Padmaja, 2017). Kavya and Padmaja (Kavya & Padmaja, 2017) detected optic disc shape and extracted using morphological procedure, red channel used and the features extracted using Gray Level Co-occurrence Matrix (GLCM) and Markov model, SVM learned from extracted features and used weights and knowledge that gained to classify correctly.

Some approaches combined structural and non-structural features to glaucoma screening as proposed in (Claro et al., 2019) that extracted structured and non-structured features, where the features were extracted using LBP, GLCM, Histogram

of Oriented Gradient (HOG), Tamura, GLRLM, morphology, and seven CNN architectures after the segmentation was performed. Thakur and Juneja (Thakur & Juneja, 2020) used two databases and extracted structured and non-structured features after performing segmentation to glaucoma identification. The features types and names of extracted techniques and classifiers were observed in Table 3.4.

Table 3.4: Different types of features and the classifiers that used in automated glaucoma detection.

Author	Used Database	Features Type	Feature Extraction Method	Classifier	Accuracy
(Nayak et al., 2009)	61 fundus images collected from the Kasturba Medical College, Manipal, India.	Structural features	CDR, ISNT ratio, distance between optic disc and center of optic nerve head.	CNN	90%
(Chrástek et al., 2005)	1100 Heidelberg retina tomograph images from Erlangen Glaucoma Registry.	Structural features	Optic nerve head size, Rim area, parapapillary atropy.	LDA, Bagging, CTREE	72%
(Shinde, 2021)	RIM-ONE v1, DRISHTI, DRIONS-DB, JSIEC and DRIVE	Structural features	CDR, ISNT ratio, blood vessels ratio	SVM, Adoboost, NN	96%
(Kavya & Padmaja, 2017)	DRISHTI	Non-structured features	GLCM, markov model.	SVM	86%
(Claro et al., 2019)	RIM-ONE v1, RIM-ONE v2, RIM-ONE v3 and DRISHTI	Structural and non-structured features	LBP, GLCM, HOG, morohology, Tamour.	SVM, Multi-layer Perceptron (MLP), RF	93%
(Thakur & Juneja, 2020)	RIM-ONE v3 and DRISHTI	Structural and non-structured features	CDR, disc damage likelihood scale, GLRLM, GLCM, First Order Statistical (FOS), Higher Order Spectra (HOS), Higher Order Cumulant (HOC) and Wavelets.	KNN, RF, SVM, NN, Naïve Bayes (NB)	93%

3.3 Preprocessing in Automated Glaucoma Detection

Preprocessing is a critical process in CAD systems, many approaches were reported their preprocessing techniques that utilized to eliminate inconsistencies and to obtain clear detailed data of an image.

CDR is the most used measurement in automated glaucoma screening that obtained by applying preprocessed techniques such as remove blood vessels (Madhusudhan, Malay, Nirmala, & Samerendra, 2011) (Nyúl, 2009) (Devasia, Jacob, & Thomas, 2019) and edge detection (Anusorn, Kongprawechnon, Kondo, Sintuwong, & Tungpimolrut, 2013). Due to the clarity of optic cup in green channel and the optic disc in red channel that motivated many studies to separate color channels of an image to achieve clear CDR (Agarwal et al., 2015) (Maheshwari, Pachori, & Acharya, 2016) (Issac, Sarathi, & Dutta, 2015), detailed data that obtained from R,G,B components was utilized in image process.

In addition, resizing the images to unified size contributed of improve the speed of image processing (Dey & Dey, 2018) (Deepak Parashar & Dheraj Agrawal, 2021).

Histogram equalization (HE) was one of the most preprocessed techniques in glaucoma detection systems that was adopted to enhancement the image due to the unified distributions of histograms and then enhancement the contrast of original images (Ayub et al., 2016) (Acharya et al., 2015) (Krishnan & Faust, 2013) (Dua, Acharya, Chowriappa, & Sree, 2011).

Other preprocessed methods such as median filter (Elseid & Hamza, 2018) and wavelet transform (Khan et al., 2021) (Deepak Parashar & Dheeraj Agrawal, 2021) (Parashar & Agrawal, 2020) that contributed in noise removing of images, that improved the image quality, where the extracted features of decomposed component improved the image classification (Deepak Parashar & Dheeraj Agrawal, 2021). Previous discussed studies of preprocessing, feature extraction and classification techniques were reported in Table 3.5.

Although, many researchers eliminated the preprocessed phase and was not utilized the techniques of image enhancement and sufficed of feature extraction and classification methods such as (Soman & Mathew, 2016) (Dey & Bandyopadhyay, 2016) (Suh et al., 2013). The applying of preprocessing techniques contributed to improve the performance of glaucoma detection as Meier, Bock, Michelson, Nyul and

Hornegger (Meier, Bock, Michelson, Nyul, & Hornegger, 2007) stated when they applied their methodology without preprocessing stage and applied same methodology with adopted blood vessels removing, illumination the correction and ROI normalization that improved the accuracy from 79% of original images to 81% of enhancement images.

Table 3.5: Preprocessing techniques and the purpose of some automated glaucoma diagnosis researches.

Author	Preprocessing Method	Feature Extraction Method	Classifier
(Madhusudhan et al., 2011)	Remove blood vessels and normalization	CDR	Multi-thresholding
(Nyúl, 2009)	Enhancement the contrast and blood vessels removing	PCA	SVM
(Devasia et al., 2019)	Separate the channels, extract ROI and remove blood vessels	ISNT, CDR	Clustering
(Anusorn et al., 2013)	Ellipse fitting and edge detection	CDR	k-mean clustering
(Agarwal et al., 2015)	Separate the image channels	Mean of CDR	Thresholding
(Maheshwari et al., 2016)	Channel extraction	Empirical Wavelet Transform	Least Square SVM (LS-SVM)
(Issac et al., 2015)	Separate the image channels	CDR	SVM and NN
(Ayub et al., 2016)	Morphological operations and HE	CDR	k-mean clustering
(Acharya et al., 2015)	HE	Gabor features	Naïve Bayes and SVM
(Krishnan & Faust, 2013)	Random transform and HE	Wavelet energy features	SVM
(Dua et al., 2011)	HE	Wavelet features	SVM, Naïve Bayes and Random forest
(Elseid & Hamza, 2018)	Median filter and channel extraction	Shape features	RUSBoost tree
(Khan et al., 2021)	Channel separation and 2D-DWT	Statistical features	LS-SVM
(Deepak Parashar & Dheeraj Agrawal, 2021)	Channel separation and ED-DWT	GLCM	KNN
(Parashar & Agrawal, 2020)	Contract limited adaptive histogram equalization (CLAHE) and 2D-LittelewoodPlaey-EWT	Entropy features	Random Forest

In addition, Sahu, Singh, Kumar, Singh and Kumar (Sahu, Singh, Kumar, Singh, & Kumar, 2019) concluded that de-noising methods improved the efficient of glaucoma detection system by improving the recognize of image data.

3.4 Segmentation in Automated Glaucoma Detection

Many researches had more attention on segmentation phase, that provided many information of eye conditions and estimated the statue of the eye. Optic disc evaluation was essential to glaucoma monitoring and detection. In optic nerve head segmentation, the optic disc was more accurate in red channel, where the optic cup was segmented accurately in green channel that made difficult to obtain accurately segmentation in same image component.

One of the challenges in development of glaucoma CAD systems was the optimal segmentation (Claro et al., 2019), in order to analysis the performance of the whole system, it was depending on the accuracies of segmentation and classification techniques.

Other feature that adopted in automated glaucoma screening was in (Costa et al., 2017) that used the vessels tree and their fundus images for glaucoma assessment, the main challenge was vessels segmentation accurately, where it proposed in (Fu, Xu, Lin, Kee Wong, & Liu, 2016) that CNN was applied to segment vessels of an eye retinal images, whereas, Carmona *et al.* (Carmona et al., 2008) performed optic nerve head segmentation of fundus images using genetic algorithm. The purpose of the previous researches and the used technique were listed in Table 3.6.

Table 3.6: Few of different researches that interested of Segmentation phase in automated glaucoma diagnosis.

Author	Data Type	Segmentation Technique	Purpose
(Carmona et al., 2008)	Fundus images	Genetic Algorithm	To locate and segment optic nerve head.
(Costa et al., 2017)	Fundus images	Adversarial Autoencoder	Vessel network segmentation
(Fu et al., 2016)	Fundus images	CNN, Conditional Random Field	Vessel network segmentation

3.5 Deep Learning in automated Glaucoma Classification

Deep learning techniques were applied widely in glaucoma identification that were adopted in optic disc and optic cup segmentation and in classification purpose. Sevastopolsky (Sevastopolsky, 2017) used U-net CNN to automate optic disc and optic cup segmentation, Bisneto *et al*. (Bisneto et al., 2020) used Generative Adversable Network (GAN) in a purpose of segment optical disc in fundus images.

In addition, Jiang, Tan and Peng (Jiang, Tan, & Peng, 2019) adapted VGG19 deep learning architecture and eight-layered CNN to semantic segmentation of optic disc and optic cup. Bajwa *et al.* (Bajwa et al., 2019) localized ROI in fundus images using Regions with CNN (RCNN), then classify glaucoma using deep CNN. Singh and Garg (Singh & Garg, 2019) used Relu activation function in CNN to perform optic nerve head segmentation. Sufficient improvement achieved in segmentation accuracy when two databases were demonstrated in (Son, Park, & Jung, 2019) when GAN segmented retinal vessels and optic disc from fundus images.

Authors (Al-Bander, Al-Nuaimy, Al-Taee, & Zheng, 2017) used CNN to extract the features that discriminant optic disc and optic cup region and used linear classifier to perform classification. The utilized techniques of previous studies and their aims were proposed in Table 3.7.

Table 3.7: Some studies that performed Segmentation phase using Deep Learning techniques.

Author	Data Type	Segmentation Technique	Purpose
(Sevastopolsky, 2017)	Fundus images	U-Net CNN	Optic cup and optic disc segmentation.
(Bajwa et al., 2019)	Fundus images	RCNN, Deep CNN	Locate optic nerve head then classify healthy and glaucoma images.
(Singh & Garg, 2019)	Fundus images	U-Net NN, CNN	Perform segmentation of optic disc and optic cup and screening glaucoma.
(Son et al., 2019)	Fundus images	GAN	Vessel segmentation, optic cup and optic disc segmentation.
(Bisneto et al., 2020)	Fundus images	GAN	Optic cup and optic disc segmentation.

Applying deep learning techniques in classification was proposed in (Cerentini et al., 2018) by training using GoogLenet network to detect glaucoma. Early and advanced glaucoma screened by applying Tensorflow CNN architecture using 1542 fundus images and increased the images by rotation to learn deep learning model. Al-Bander *et al.* (Al-Bander et al., 2017) combined 23 layered CNN and SVM to detect glaucoma with RIM-ONE version2 and obtained 88.2% accuracy value.

Deep learning became an emerging technology in many ophthalmology applications, where deep learning techniques were adopted to identify glaucoma using small set of images as proposed in (Chen, Xu, Yan, et al., 2015) (Chen, Xu, Wong, Wong, & Liu, 2015) (Raghavendra et al., 2018), to prevent the overfitting they limited the number of layers which caused the limitation in the network ability to learn specific features.

To overcome the problem of small size of databases and overfitting (Al Ghamdi, Li, Abdel-Mottaleb, & Abou Shousha, 2019) proposed supervised and unsupervised learning methods to learn using labeled and unlabeled data by combining transfer learning and self-learning in proposed approach (Salam, Khalil, Akram, Jameel, & Basit, 2016).

Transfer learning is a machine learning technique that applyed to develop model of previous tasks in a new task domain (An et al., 2019) that used as an alternative solution when CNN was not usable, by using pre-trained CNN that trained on millions of images of thousands of classes. Combined information of macular area in OCT and optic disc in fundus images was proposed to identify glaucoma by (An et al., 2019) using transfer learning of VGG19 CNN architecture (by 19 layers) to extract the features to train RF classifier.

Authors (Gómez-Valverde et al., 2019) Introduced different CNN architectures because of successful in medical image analysis, with transfer learning which used for pre-trained CNN architectures while three datasets were used. The method accuracy achieved to 94%. The large number of architectures made the learning process complicated and took long time to learn.

The authors in (Serener & Serte, 2019) applied transfer learning and deep learning techniques to classify glaucoma to early or advanced glaucoma using fundus images, after preprocessing the classification was done using fifty layers of ResNet and GoogLeNet. Transfer learning was applied to detect two classes of glaucoma severity. The accuracies were 90% for early glaucoma and 85% for advanced glaucoma.

Pinto *et al.* (Diaz-Pinto et al., 2019) addressed the problem of small database and using CNN to train small-labeled database and large unlabeled database. Deep Convolutional Generative Adversarial Network (DCGAN) semi-supervised learning method provided labels to unlabeled data, the accuracy of this approach reached to 90%. Al Ghamdi, *et al.* (Al Ghamdi et al., 2019) presented a method for both supervised and unsupervised learning. In the first stage, labeled data was used to train the CNN classifier then unlabeled data was used to increase the dataset and used in training to avoid overftting. Method accuracy was 92%, although unlabeled data contributed to achieve high accuracy, but also the training time increased because of the increasing in the number of iteration.

Finally, Deep Learning techniques had been used in (de Sales Carvalho et al., 2021) to automated glaucoma diagnosis using retinal images without optic disc segmentation. The approach adapted three-dimensional Convolutional Neural Network (3DCNN). Firstly, the images were acquired by RIM-ONE and Drishti-GS databases, followed by transform images from 2D to volumetric images to extract non-human perceivable attributes using 3DCNN although the high cost of entire technical and computational process.

CNN architectures consumed large database and computational power to define the size, quantity and layers configuration, where the performance of the network depended on the diversity and the amount of used images, the deep learning techniques were good as inputted images are good. In addition, the features were mapped during the training time without explanation why the image was classified normal or glaucoma, where the black box of deep learning considered drawback in medical diagnosis that was a critical issue to understand the result (Ahn et al., 2018). Table 3.8 listed some studies that performed automated glaucoma classification using Deep Learning techniques.

Table 3.8: Some studies that perform automated glaucoma classification using Deep Learning techniques.

Author	Data Type	Classifier	Purpose
(Chen, Xu, Wong, et al., 2015)	2726 Fundus images	CNN	Glaucoma detection.
(Chen, Xu, Yan, et al., 2015)	2726 Fundus images	6-layers CNN	Glaucoma screening based of extracted features of CNN.
(Raghavendra et al., 2018)	1426 Fundus images	18-layers CNN	Automated glaucoma detection based on deep learning approach.
(An et al., 2019)	357 OCT and Fundus images	VGG19 architecture	Classify images using transfer learning of CNN.
(Al-Bander et al., 2017)	455 Fundus images	CNN	Classify glaucoma images based on extracted features of CNN
(Gómez-Valverde et al., 2019)	2313 fundus images	Transfer learning with VGG19	Detect glaucoma in retinal fundus images.
(Serener & Serte, 2019)	7118 Fundus images	GoogLeNet Deep CNN	Detect early and advanced open angle glaucoma using fundus images.
(Diaz-Pinto et al., 2019)	86926 labeled and unlabeled fundus images	DCGAN	Automated glaucoma assessment using semi-supervised classification.
(Al Ghamdi et al., 2019)	1955 fundus images.	Semi-Supervised Transfer Learning CNN.	Use labeled and unlabeled data to increase the performance of CNN to detect glaucoma.
(de Sales Carvalho et al., 2021)	556 Fundus images	3D-CNN	Classify glaucoma images without optic nerve head segmentation.
(Krishnamoorthi & Chinnababu, 2019)	330 Fundus images.	SVM, Naive Bayes (NB) and Logistic Regression (LR)	Investigate retinal images by using non-morphological features to detect glaucoma.
(Ahn et al., 2018)	1542 Fundus images	CNN	Detect early and advanced glaucoma.

Following, the research presented various methodologies of automated glaucoma identification that had a high performance and applied similar approach of our work in a manner of type of data, classification purpose and features type.

The great work was presented in (Krishnamoorthi & Chinnababu, 2019) to detect glaucoma from retinal images using three public datasets with three classifiers. Authors extracted non-morphological features using LBP, HOG, and fractal analysis. The model accuracy achieved to 91%. The features were combined to improve the performance, Sequential Floating Forward Selection (SFFS) was used for features selection. Three classifiers were applied to learn models SVM, NB, and LR to detect glaucoma. The highest accuracy was achieved when hybrid features were used by a combination of LBP and fractal analysis features.

The method proposed in (Bisneto et al., 2020) divided into image acquisition from two public datasets, trained for optic disc segmentation using Generative Adversarial Network (GAN), extracted texture attributes through Taxonomic Diversity, finally classification through three classifiers MLP, Sequential Minimal Optimization (SMO) and Random Forest. Firstly, the accuracy was limited but after contrast enhancement technique was applied on test set images, the accuracy improved. The used database was labeled based on image characteristics without clinical information, which lacked the reliability of the proposed method.

Chaudhary and Pachori (Chaudhary & Pachori, 2021) attempted to preprocess images using CLAHE, and decomposition green channel using two Dimensional Fourier-Bessel Series Expansion based Empirical Wavelet Transform (2D-FBSE-EWT) method to images enhancement, followed by using GLCM, chip features and invariant moment features methods to extract a feature vector from sub-images that described shape, position and orientation of an image. Two approaches were performed for classification machine learning approach using SVM, MLP, LS-SVM, RF and deep learning approach, that applied on RIM-ONE, Drishti-GS and ORIGA databases.

Claro *et al.* (Claro et al., 2019) presented automated approach to classify glaucoma using texture and CNN descriptors. When six categories of feature extraction methods namely, HOG, GLCM, LBP, Tamura, GLRLM, morphology and seven CNN architectures used to determine the best collection of features that classified retinal images in a term of homogeneity and heterogeneity of optic disc and optic cup color,

cup region and thickness of vessels. About 1675 fundus images were used and 30682 features were extracted.

Thakur and Juneja (Thakur & Juneja, 2020) proposed methodology that combined structural and non-structural descriptors. The segmentation was performed using Level set based Adaptively Regularized Kernel based Intuitionistic Fuzzy C Means (LARKIFCM), followed by ranking the extracted non-structured features by applied GLCM, GLRLM, FOS, HOS, HOC and DW from grayscale fundus images of RIM-ONE and Drishti-GS databases.

The proposed approach in (Khan et al., 2021) classified health and pathological retinal image. Firstly, the authors applied 2D-DWT denoising technique on fundus images, statistical features were extracted and feed to LS-SVM classifier.

De Sousa *et al.* (de Sousa et al., 2017) extracted textural features to glaucoma diagnosis in 455 retinal images using SVM and genetic algorithm as classifiers. Where geostatistical functions (semivariogram, semimadogram, covaripgram and correlogram) described texture features from optic disc region that represented by LBP.

De Carvalho Junior *et al.* (de Carvalho Junior et al., 2018) were performed segmentation on RIM-ONE and Drishti-GS databases images using Otsu and k-means methods to delimit optic disc region. Therefore, the authors extracted statistical properties of texture based on phylogeretic diversity indexes, which metric calculated population diversity. The applied classification methods were RF, MLP, NN and SMO.

The imbalanced data issue in glaucoma detection was presented by (Zhao et al., 2022) that divided the data to imbalanced class and rare cases, which led to produce model dominated by majority cases. Zhao *et al.* (Zhao et al., 2022) proposed an adaptive strategy to re-balancing data using self-ensemble dual-curriculum learning by distilling the features and reweighting the imbalance data to obtain optimal boundary for detect glaucoma accurately. The approach was evaluated on LAG, REFUGE and RIM-ONE databases.

3.6 Summary

Review related automated glaucoma detection studies were important to identify used techniques, features and to identify the gab in the research field, where more effort in automated glaucoma identification is required to develop the performance of disease detection as stated in (An et al., 2018).

Firstly, many measurements and retinal image modalities were used, this work selected fundus image as data type to train our model due to its availability and the low cost compared to OCT that was advanced image modality but not popular and with high cost. In addition, fundus images had public available databases that were used in abundance automated glaucoma screening compared to visual field data.

Preprocessing was an important stage that contributed to removing unnecessary inconsistencies in the image such as poor contrast and light, also it contributed to improve the recognition of more additional data in images, which improved the performance of automated diagnosis of glaucoma (Sahu et al., 2019).

In addition, many studies were concerned only on optic nerve head segmentation, delimiting optic disc and optic cup and its relationship with glaucoma through the diameter calculation need to evaluation to detect its accuracy. The errors in segmentation caused due to the low contrast among optic disc and background, color similarity and low variation in fundus images of retina (Claro et al., 2019).With extract non-morphological features, the segmentation process was eliminated, also researches that used non-morphological features had accuracy higher than that used morphological features .

Due to small size of available public databases of retinal images, using deep learning techniques were challengeable task. In addition, the low quality of fundus images made difficult to extract features or learn using DL.

This research focused to enhancement the performance of automated glaucoma screening by providing significant features of fundus images to glaucoma classification by using combination of two features extracted methods to obtain non-structured parameters, followed by adapting features reduction technique to obtain discriminant features vector to enhance models construction using two classifiers to evaluate the features and classify glaucoma images.

CHAPTER FOUR

Methodology

Chapter three reviewed many studies that aimed to detect glaucoma using machine learning techniques where the researchers studied the automated glaucoma diagnosis from different aspects and using multiple types of data. In this section, the proposed methodology was introduced for classifying glaucoma and healthy images using non-structured features by representing images and recognize a certain pattern. The proposed methodology was organized to five steps as represented in Figure 4.1.

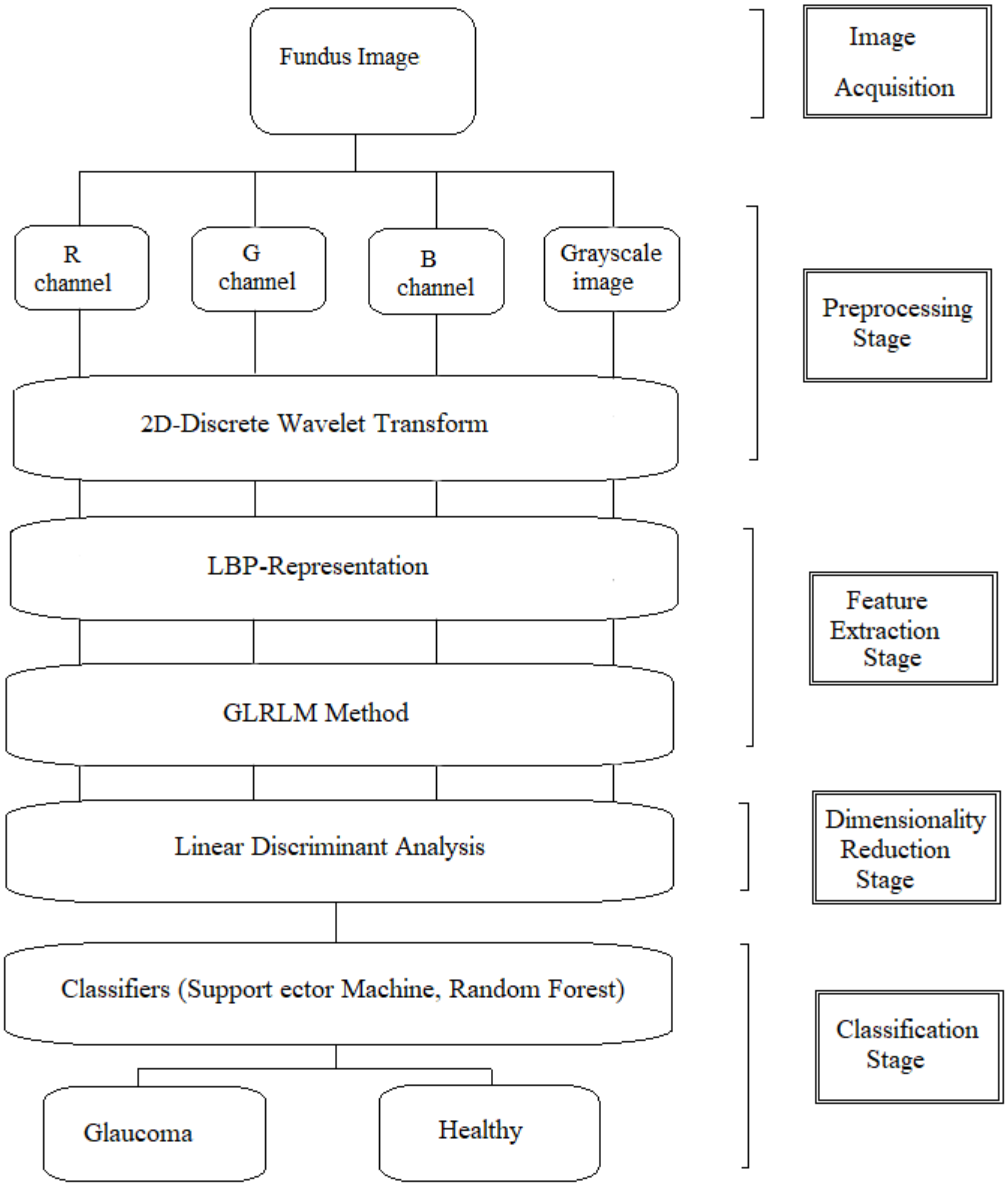

Figure 4.1: The methodology of the proposed approach.

4.1 Image Acquisition

Many databases were used in reviewed studies, our methodology used public database to compare our results with related studies that used same database and given a chance to other researchers to verify with our approach.

Table 3.3 observed the versions of RIM-ONE database that were the most relevance to use due to the size and reliable diagnosis of their images through specialists.

The images were read from public RIM-ONE databases (Fumero et al., 2011). Open Retinal Image database for Optic Nerve Evaluation (RIM-ONE) database was a group of databases (versions) that contained healthy and ophthalmic images as presented in Table 4.1. The database images were designed for glaucoma diagnosis with normal and glaucoma labels. In addition, it was designed as an evaluation tool for segmentation algorithms, where it had a manual segmentation reference for each image performed by ophthalmic experts.

Table 4.1: The number of images in RIM-ONE database Versions.

RIM-ONE Version	No. Glaucoma Images	No. Normal Images	Type	Size
V1	51	118	bmp	Different
V2	200	250	jpg	Different
V3	74	85	jpg	2144 x 2144

The images of RIM-ONE version1 (V1) and version2 (V2) were acquired using Nidek AFC-210 retinal fundus camera under different contrast and brightness conditions. However, RIM-ONE version3 (V3) images were taken by Kowa WX 3D stereo camera that took two images of retina from different angles with high resolution that made one of the automated detection challenged of capturing images with different cameras and professionals. It is worth mentioning that glaucoma images in RIM-ONE V1 contained early glaucoma images in the first stage, which were difficult to distinguish.

4.2 Preprocessing

Enhancement the input image for further processing as a pattern recognition by eliminating the noise was a critical step, where many reasons effected on fundus image as space radiation, impulsive noise (Yu, Ma, Zheng, & Liu, 2016), that had negative effect during acquisition and transmission image. Image de-noised attempted to remove noise or artifacts from an image, which resulted de-noised image.

Firstly, the stereo fundus images of V3 of RIM-ONE database were cropped to (2144 x 1424) to obtain one fundus image. The input images of V1 and V2 and V3 of RIM-ONE database were resized to (512 x 512) for normalization purposes, for each image, four images were obtained by separating image channels into (R, G, B) plans, and obtained grayscale image of input image. In purpose of de-noising, the R, G, B components and grayscale images were decomposed to various frequencies using 2D-DWT algorithm to eliminate the noise and obtain clear image.

2D-Discrete Wavelet Transform (2D-DWT):

2D-Discrete Wavelet Transform (2D-DWT) technique was used to enhancement the images by performing the de-noising. Instead of using the whole image (signal), DWT separated the image to smaller components (Sub-bands) then processing these components was simpler. 2D-DWT was applied on R-G-B channels, and grayscale images as shown in Figure 4.2, begin with additive white Gaussian (speckle) noise to all pixel values in each image.

Each image decomposed to four sub-bands, which were Low-Low (LL), Low-high (LH), High- Low (HL) and High-High (HH) using 2D-analysis filter bank, where first stage of filter bank applied on the image columns to obtain (L,H) sub-bands. In the second stage, the filter bank applied on each row in the 2 sub-bands to obtain the four sub-band images as in Figure 4.3. 2D-DWT implemented by repeating the decomposition process by applying 2D filter bank on the low sub-band (LL) based on the number of stages. The most image information was available in low frequency (LL) approximation. HH had dialog details of image and noisy data information. The horizontal and vertical details existed in LH and HL, respectively (Sahu et al., 2019).

DWT was applied to transform noisy image into an orthogonal domain. Signal parameter, signal variance and noise variance were used by bayes estimator to estimate coefficient with free noise using bivariate shrinkage function that performed on LL

sub-band coefficients. Reconstruct de-noised image by computing Inverse DWT (IDWT) using modified coefficients (Şendur & Selesnick, 2002).

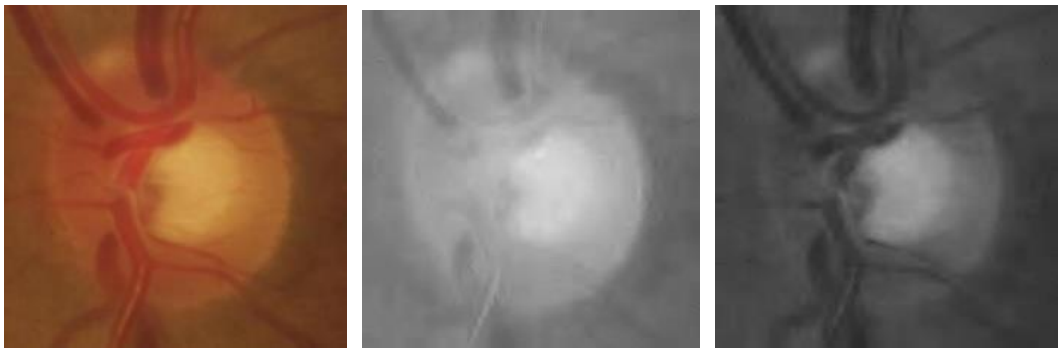

Input image Red image Green image

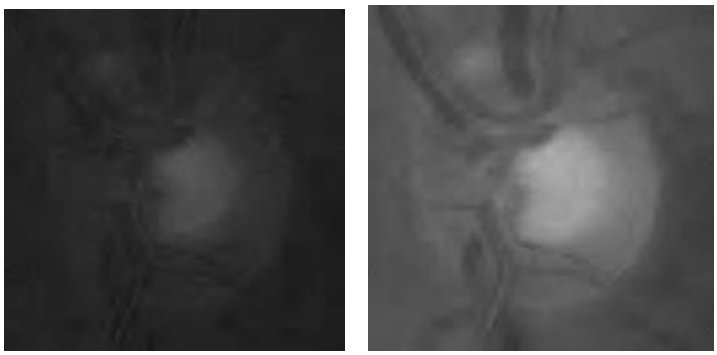

Blue image Grayscale image

Figure 4.2: Original input image and resulted de-noising R-G-B channels/grayscale images using 2D-DWT.

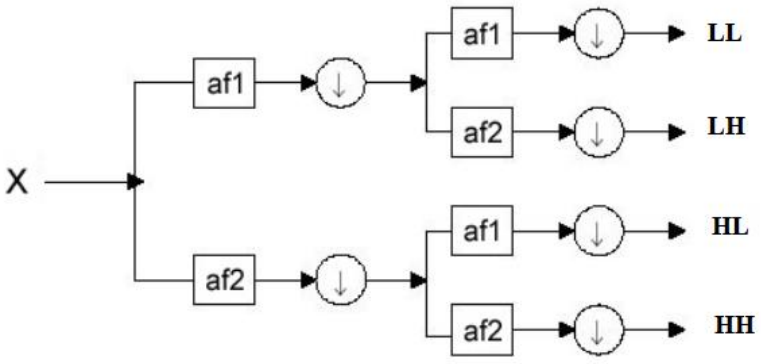

Figure 4.3: One stage in 2D filter bank of DWT decomposition.

The de-noising process as follow:

1. Calculate the noise variance using median estimator.
2. Calculate the 2D-DWT of an image and obtain wavelet coefficient.
3. For each wavelet coefficient 7x7 block calculate:
    a) Calculate noisy coefficient.
    b) Compute signal variance estimation.
    c) Use bivariate shrinkage to estimate each clear wavelet coefficient.
4. Calculate inverse 2D-DWT from cleared wavelet coefficient.

Segmented optic disc area from fundus images was a relevant task and helped to assess glaucoma damage of optic nerve head. But in non-morphological features, the image segmentation process was not needed to extract features like color, shape, and texture that could capture from existing images, although manually segmentation was applied on optic nerve head images in proposed datasets by five experts to be as a reference for glaucoma images segmentation and classification purpose.

4.3 Feature Extraction

Feature extraction methods aimed to describe an image using extracted attributes that used to recognize a pattern and employed to make an accurate decision during classification. Non-structural features were obtained from preprocessed (R, G, B, and grayscale) images after representing the images by performing LBP method, followed by extract 16 features from each image by applying GLRLM method on them. The methods were explained as followed:

4.3.1 Local Binary Pattern (LBP)

LBP is a simple method to describe a local image pattern and was adapted in many applications and had impressive results such as face recognition (Ahonen, Hadid, & Pietikäinen, 2004) and shape localization (X. Huang, Li, & Wang, 2004). LBP represented local features of an image by providing information of a local difference and provided a binary presentation of an image texture, which also represented the image shape (Guo, Zhang, & Zhang, 2010). LBP reflected the functionality of the algorithm where the local neighborhood was the threshold at the gray level of the central pixel into a binary pattern.

LBP was applied on each pixel in an image, the image splitted to 3x3 block, where it provided better performance than any other methods, the pixels in each block were threshold using the center pixel as presented in Figure 4.4.

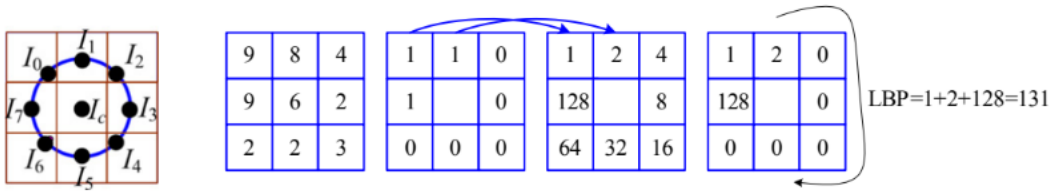

(a) (b)

Figure 4.4: shows (a) central pixel and its neighbor, (b) LBP computing.

The value of the neighborhood pixel was determined depending on a center pixel value, where if neighborhood value was lower than center pixel value, then pixel value got zero value. Otherwise, it was assigned as one. The vector of eight neighborhood pixels was multiplied by two power pixel position in block in a clockwise direction. The results were binary numbers as shown in Figure 4.5.

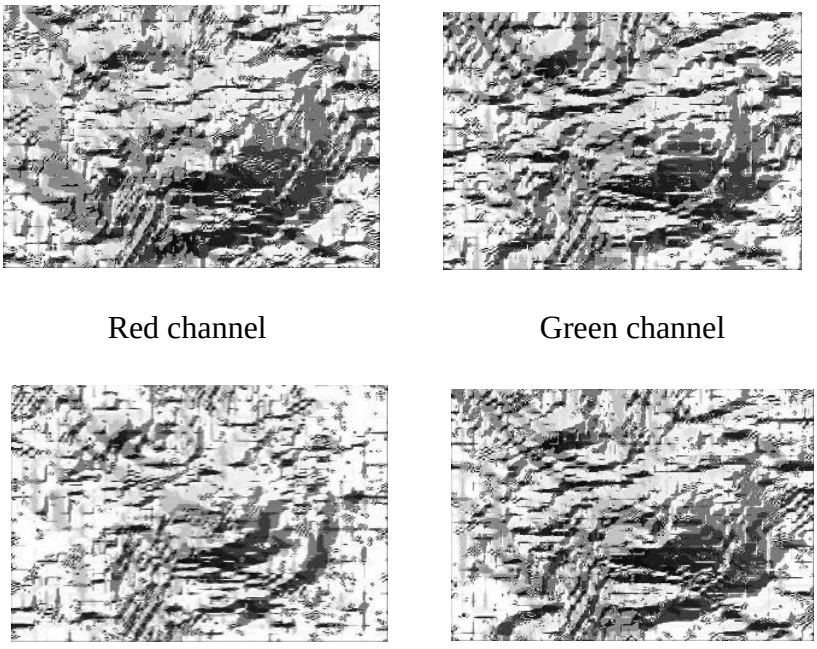

Red channel Green channel

Blue channel Grayscale image

Figure 4.5: LBP-representation of R-G-B channels and grayscale image.

LBP descriptor is an efficient invariant texture, which integrates structural and statistical texture features. Usually, histogram features (mean, standard deviation, entropy, energy, variance, skewness, and kurtosis) as in (Krishnamoorthi & Chinnababu, 2019) (Romany F. Mansour & Al-Marghilnai, 2021) (Srinivasan, Dubey, & Ganeshbabu, 2016) were extracted from LBP representation of an image. GLRLM method was employed to extract features from LBP representation.

LBP is an efficient and simple computing technique that was demonstrated in many fields as shape localization (Kadlček & Fucik, 2012) and face recognition (Suruliandi, Meena, & Rose, 2012), and provided a high discriminative texture property, invariance to monotonic changes of gray level and it preserved the intensity order of neighborhood pixels (Krishnamoorthi & Chinnababu, 2019) that advantages made LBP relevance technique to reflect the local neighborhood pixels functionality.

4.3.2 Gray Level Run-Length Matrix Method (GLRLM)

Various texture features were used to detect glaucoma such as GLCM, GLRLM, etc. GLRLM proposed firstly by Galloway in 1975 (Galloway, 1975) as a matrix that aimed to describe texture features of an image using auxiliary matrices by counting the repetition of gray level pixel and in which direction. Run length means the string of consecutive pixels that have equally gray level intensity, which locates in a specific linear orientation. GLRLM evaluated the spatial distribution of gray level values, by calculating a set of descriptors from local characteristics distributions (Chu, Sehgal, & Greenleaf, 1991) (Dasarathy & Holder, 1991).

Gray level run described a set of co-linear and successive pixels with the same value of gray level, each element in a matrix represented by calculating the line of pixels that had equal intensity values and in a certain direction (0^{o} corresponding to horizontal, 45^{o} diagonal direction, 90^{o} represent the vertical direction and 135^{o}). The produced matrix was the mean of four direction matrices.

The following example in Figure 4.6 presented (4x4) matrix that had (0–3) four gray level and produced GLRLM for four directions (0^{o}, 45^{o}, 90^{o}, 135^{o}).

Usually short runs with similar gray level intensity located mostly in fine textures, while the coarse texture tend to had long runs with different gray level intensity (Galloway, 1975). Extracted descriptors viewed the whole characteristics of an image, for example Run Percentage (RP) measured the distribution and homogeneity of runs

of an image in specific direction. While Short Run Emphasis (SRE) measured short runs distribution of an image.

(4x4) matrix

0	1	2	3
0	2	3	3
2	1	1	1
3	0	3	0

GLRLM matrix in 0º direction

Run Length

gray level	0º	1	2	3	4
	0	4	0	0	0
	1	1	0	1	0
	2	3	0	0	0
	3	3	1	0	0

GLRLM matrix in 45º direction

Run Length

45º	1	2	3	4
0	4	0	0	0
1	4	0	0	0
2	0	0	1	0
3	3	1	0	0

GLRLM matrix in 90º direction

Run Length

90º	1	2	3	4
0	2	1	0	0
1	4	0	0	0
2	3	0	0	0
3	3	1	0	0

GLRLM matrix in 135º direction

Run Length

135º	1	2	3	4
0	4	0	0	0
1	4	0	0	0
2	3	0	0	0
3	5	0	0	0

Figure 4.6: presents how to calculate GLRLM of (4x4) matrix for four directions (0º, 45º, 90º, 135º).

Run length features had not been demonstrated extensively in texture analysis and pattern recognition compared to traditional texture features as GLCM, spatial gray level dependence, etc. Although new features were obtained from run length matrix

until 1991 (Dasarathy & Holder, 1991). In CAD systems of glaucoma detection, GLRLM method considered an uncommon feature extracted method. To the best of our knowledge, two studies were extracted statistical features using GLRLM to detect glaucoma (Thakur & Juneja, 2020) (Claro et al., 2019). In (Thakur & Juneja, 2020), just five features were extracted and due to feature ranking, GLRLM features were not involved in the feature vector that adapted for classification.

Where in (Claro et al., 2019), eleven features were extracted from GLRLM method without preprocessing the images, which caused the low performance of the method. The first extracted features of GLRLM were proposed by Galloway in 1974, that were five measures (Galloway, 1975). In 1990, two further features were denoted in (Chu, Sehgal, & Greenleaf, 1990), followed by other four descriptors were discovered by Dosarathy and Holder in 1991 (Dasarathy & Holder, 1991), and the normalized values of two features (gray level non-uniformity normalized and run length non-uniformity normalized) were added with calculated gray level variance, run variance, and run entropy that provided by radiomic library (Van Griethuysen et al., 2017). The description of GLRLM features was stated as following:

P(M,N) is a run length matrix, each $P(i,j)$ represent the number of runs with pixels of gray level value (intensity) equal to i and run length equal to j along specific direction. (n_r) is the number of runs in the image, and $p(i,j)$ is the normalized run length matrix.

The features of GLRLM were calculated such as:

1- Short Run Emphasis (SRE) computed the short runs distributions. It had a large value with fine textures.

$$SRE = \frac{1}{n_r} \sum_{i=1}^{M} \sum_{j=1}^{N} \frac{p(i,j)}{j^2}$$

2- Long Run Emphasis (LRE) computed the long runs distributions. It had a large value with roughness structural textures.

$$LRE = \frac{1}{n_r} \sum_{i=1}^{M} \sum_{j=1}^{N} P(i,j) * j^2$$

3- Low Gray-Level Run Emphasis (LGRE) computed the low gray level values distributions. It had a large value with image that has low gray level values.

$$LGRE = \frac{1}{n_r} \sum_{i=1}^{M} \sum_{j=1}^{N} \frac{p(i,j)}{i^2}$$

4- High Gray-Level Run Emphasis (HGRE) computed the high gray level values distributions. It had a large value with image that has high gray level values.

$$HGRE = \frac{1}{n_r} \sum_{i=1}^{M} \sum_{j=1}^{N} P(i,j) * i^2$$

5- Short Run Low Gray-Level Emphasis (SRLGE) computed the combination of short runs and low gray level values distribution. It had a large value with image of lower values of gray level and many short runs.

$$SRLGE = \frac{1}{n_r} \sum_{i=1}^{M} \sum_{j=1}^{N} \frac{P(i,j)}{i^2 * j^2}$$

6- Long Run Low Gray-Level Emphasis (LRLGE) computed the combination of long runs and low gray level values distribution. It had a large value with image of lower values of gray level and many long runs.

$$LRLGE = \frac{1}{n_r} \sum_{i=1}^{M} \sum_{j=1}^{N} \frac{P(i,j) * j^2}{i^2}$$

7- Short Run High Gray-Level Emphasis (SRHGE) computed the combination of short runs and high gray level values distribution. It had a large value with image of higher values of gray level and many short runs.

$$SRHGE = \frac{1}{n_r} \sum_{i=1}^{M} \sum_{j=1}^{N} \frac{P(i,j) * i^2}{j^2}$$

8- Long Run High Gray-Level Emphasis (LRHGE) computed the combination of long runs and high gray level values distribution. It had a large value with image of higher values of gray level and many long runs.

$$LRHGE = \frac{1}{n_r} \sum_{i=1}^{M} \sum_{j=1}^{N} P(i,j) * i^2 * j^2$$

9- Gray-Level Non-Uniformity (GLNU) computed the gray level values similarity in the image. It had a large value if the image had a similar gray level values.

$$GLNU = \frac{1}{n_r} \sum_{i=1}^{M} \left(\sum_{j=1}^{N} P(i,j) \right)^2$$

10- Gray Level Non-uniformity Normalized (GLNN) was a normalized version of GLNU formula.

11- Run Length Non-Uniformity (RLNU) computed the length of runs similarity in the image. It had a large value if the image had similar run lengths.

$$RLNU = \frac{1}{n_r} \sum_{j=1}^{N} \left(\sum_{i=1}^{M} P(i,j) \right)^2$$

12- Run Length Non-uniformity Normalized (GLNN) was a normalized version of RLNU formula.

13- Run Percentage (RP) computed the distribution and the homogeneity of runs in determined direction in an image. It had a large value if the run lengths value equal to one in all gray level values in determined direction.

$$RP = \frac{n_r}{P(i,j)*j}$$

14- Gray Level Variance (GLV) computed the gray level intensity variance of the runs.

$$GLV = \sum_{i=1}^{M} \sum_{j=1}^{N} p(i,j|\theta)(i-\mu)^2$$

15- Run Variance (RV) computed the runs variance in the run lengths.

$$RV = \sum_{i=1}^{M} \sum_{j=1}^{N} p(i,j|\theta)(j-\mu)^2$$

16- Run Entropy (RE) computed randomness in the gray level values and run lengths distribution. If it had a large value that indicated to heterogeneity in the texture patterns.

$$RE = -\sum_{i=1}^{M} \sum_{j=1}^{N} p(i,j|\theta) \log_2(p(i,j|\theta) + \varepsilon)$$

The less effected by grayscale changes, preserved the intensity order of pixel, and illuminated the variant changes were strengths of LBP, whereas GLRLM method evaluated the spatial distribution of gray level values by calculating a set of statistics from local characteristics distributions and observed the coarseness of the texture in specific direction that motivate us to use this methods in proposed methodology.

4.4 Feature Reduction

It considered important step to improve the efficiency of classifiers performance. The feature reduction aimed to increase the classification performance by reducing the computational time and complexity of building the model.

Linear Discriminant Analysis (LDA):

LDA is a supervised and unsupervised machine learning technique that used as reducing dimensionality, classification, and interpretation of the significant features tool. LDA aimed to maximize the distance among classes and minimize the variance of interclass in a term of mean and variance (Ghassabeh, Rudzicz, & Moghaddam, 2015). The extracted feature vector of images and their labels were provided to LDA method. Firstly, LDA performed min-max normalization followed by computing

features that had the best discriminant among classes, where LDA method identified the most significant features and obtained linear feature combination which described the largest mean value between class (Xanthopoulos, Pardalos, & Trafalis, 2012).

4.5 Classification

In order to build robust system, each version of RIM-ONE database was evaluated separately, the features that extracted from methods in sections 4.3.1 and 4.3.2 used to train two classifiers SVM and RF classifiers, 70% of images used for training and 30% were used for testing.

4.5.1 Support Vector Machine (SVM)

SVM is administrated as non-linear solution for regression and classification problems. The supervised SVM classifier aimed to separate unseen data of the testing set using line with maximum distance (mergin) between different classes data, where mergin considered as the classes boundary. The line in a middle of mergin distance (hyperplane) must had the least possible separation error among data and the maximum distance to the closest class data.

The maximum distance among the mergins determined the best hyperplane, the optimal hyperplane aimed to enhance the generalization ability. The chosen data as a boundary of the class was termed as support vectors (Gholami & Fakhari, 2017) as in Figure 4.7.

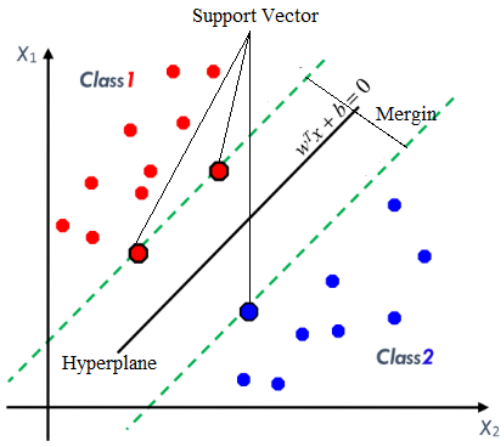

Figure 4.7: Mergins and hyperplane to classify the data to two classes in linear Support Vector Machine.

Causing of the similarity of attributes of the database, probably the data was not separated linearly, kernel functions used to perform linear and non-linear classification.

SVM had ability to learn from small set of features and databases (Gholami & Fakhari, 2017) and it considered sufficient computational technique compared to other machine learning techniques such as deep learning (Martínez-Ramón & Christodoulou, 2005) (Wang, 2005). With available small databases in glaucoma, SVM considered appropriate classifier to learn from that data. In addition, the comparison performance of our extracted features with related researches that applied SVM to build their models using same classifier was available due to SVM was commonly used in automated glaucoma field (Claro et al., 2019) (Krishnamoorthi & Chinnababu, 2019) (Chaudhary & Pachori, 2021) (de Sousa et al., 2017) (Thakur & Juneja, 2020).

4.5.2 Random Forest (RF)

RF is multiple supervised machine learning technique that constructed of collection of decision trees. Each tree was built using random samples of training data using random features, not all features constructed the tree. To perform prediction, attributes of testing set are inputted to all random tree where each tree produces unit vote for the most class probability and performs majority voting for results to obtain the class of data. The mergin measures the average number of votes, the correct class is the largest voting of other classes.

Random attribute selection contributed to reduce the correlation between trees, where all trees acted similarly if all attributes constructed the trees. Significant accuracy obtained resulting from growing the trees and letted that trees voting for appropriate class (Breiman, 2001).

Due to using samples that were not used same data for all trees, the RF considered less sensitive to training data and that made it resisted the overfitting as more trees added. In addition, the simplicity of construct RF model and its robust against the outliers made RF relevance classifier to use.

When the function error decreased significantly, and very promising results were obtained in training phase, but a poor estimation in the testing phase was achieved that termed as overfitting.

We employed supervised methods to perform glaucoma identification where pre-defined inputs were adapted to learn classifiers. The discriminant features of LDA were fed into a classifier to detect normal and abnormal cases. The effectiveness of SVM and RF classifying had been proved in related literature of glaucoma detection (de Sousa et al., 2017) (Chaudhary & Pachori, 2021), which motivated us to use them and compared the results which classifier had a high performance.

To evaluate our methodology performance, accuracy, sensitivity and specificity were metrics that had been applied to attain classification accuracy, the metrics were calculated using confusion matrix that consists of:

TP referred to number of diseased retinal images that classifier predicted as diseased.

FP referred to number of diseased retinal images that classifier predicted as healthy.

TN referred to number of healthy retinal images that classifier predicted as healthy.

FN referred to number of healthy retinal images that classifier predicted as diseased.

Sensitivity is the probability of glaucoma occurrence to the total number of glaucoma occurrence, given as bellow:

$$\text{Sensitivity} = \frac{TP}{TP+FN}$$

Specificity is the probability of non-glaucoma occurrence to the total number of non-glaucoma occurrence, given as bellow:

$$\text{Specificity} = \frac{TN}{TN+FP}$$

Accuracy is the ration between the number of correctly classified cases to the total number of all cases.

$$\text{Accuracy} = \frac{TP+TN}{TP+TN+FN+FP}$$

Python 3.7 version programming language was used to develop the algorithms, while the used machine runs on Windows 10 operating system, hardware of 64 bit Core I7 processor and RAM of 8 GB.

4.6 Summary

The proposed approach was summarized as obtaining images from public fundus images database that called RIM-ONE database. The database images were resized, separated to R-G-B channels and grayscale image and de-noised using 2D-DWT.

The enhancement images were converted to binary representation using LBP followed by extracting statistical features using GLRLM method. The features were normalized and reduced using LDA followed by using the produced features vector to train the SVM and RF classifiers.

CHAPTER FIVE

Results and Discussion

Our methodology, the performance of extracted features and used classifiers were discussed in this section. The three versions of RIM-ONE database were evaluated separately. Each version was divided into 70% of training and 30% for testing using the split method without overlapping among training and testing sets. LDA reduction technique was provided by extracted features to produce discriminant vector. SVM and RF classifiers were applied to analyze the extracted features and train the models. To evaluate the performance of classifiers, accuracy, sensitivity, and specificity were metrics that had been applied to attain classification accuracy.

Three experiments were performed to obtain the satisfied classifier performance results by obtaining the highest accuracy.

5.1 First Experiment: Combination of LBP and GLRLM without Preprocessing:

As it noted from Figure 5.1 that was different of proposed methodology in Figure 4.1 in preprocessing stage, where in this experiment, the preprocess method was not applied on the images, the images just were resized to 512x512 unified size and obtained grayscale image from color input fundus images.

The other difference was extract seven statistical features of binary LBP representation and combined them to GLRLM features instead of applying GLRLM method on binary LBP representation directly as in Figure 4.1.

First experiment involved applied LBP descriptor and GLRLM method on original images without applying preprocessing method as research proposal was proposed. The input RGB images in database were resized to 512x512 unified size followed by convert RGB images to grayscale images without applied any noise removing technique. LBP descriptor was performed on grayscale image to obtain LBP representation image, followed by compute seven statistical histogram features of represented image which were mean, standard deviation, variance, energy, entropy, kurtosis and skewness.

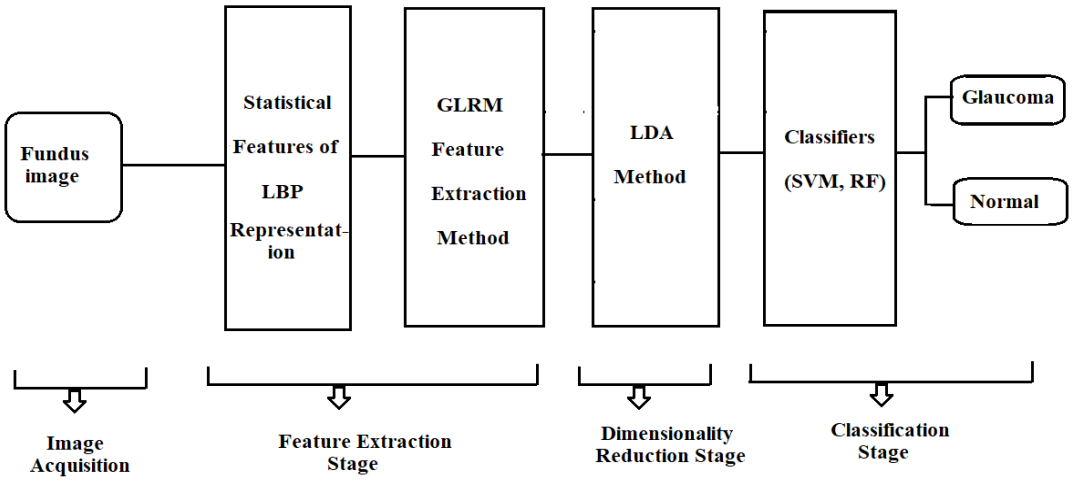

Figure 5.1: The methodology of Combination of LBP and GLRLM without preprocessing.

GLRLM method also was applied on grayscale image and obtained four matrices in each direction (0º, 45º, 90º, 135º). The sixteen gray level variance features in section 4.3.2 were computed form average GLRLM matrix of the four matrices. The features described the distribution of run length and gray level from average matrix of the four produced matrices.

The features that extracted from LBP and GLRLM methods were combined in one vector that represent an image, LDA method was applied on extracted features of LBP, GLRLM methods and the combination features of the two methods to obtain discriminant feature vectors that used to train the models of linear, polynomial SVM and RF classifiers.

The results of V1 of RIM-ONE database were listed in Table 5.1. From Table 5.1, it noted that the results of using GLRLM features to train the three classifiers were more accurate than the results of statistical features of LBP descriptor, where the linear SVM had the highest performance compared to polynomial SVM and RF with Ten-fold cross-validation.

After combine the LBP histogram and GLRLM features of each image, the performance of the three classifiers were little improved, the highest result was 84% with linear SVM classifier with Ten-fold cross-validation.

Table 5.1: The results of RIM-ONE (V1) database using SVM and RF classifiers in First Experiment.

Feature Extraction Method	Classifier	Kernel	Sensitivity	Specificity	Accuracy	Cross-validation Accuracy
GLRLM	SVM	Linear	50%	97%	82%	79%
		Polynomial	25%	100%	76%	78%
	RF		37%	80%	66%	71%
LBP	SVM	Linear	6%	100%	70%	74%
		Polynomial	6%	100%	70%	72%
	RF		31%	91%	72%	69%
LBP + GLRLM	SVM	Linear	62%	100%	88%	84%
		Polynomial	73%	80%	80%	81%
	RF		50%	76%	76%	76%

The results were not promising when the extracted features methods applied on unprepossessing data, as noted of the low performance of LBP histogram and GLRLM features each one alone, and after perform combining of the features, where the models failed to distinguish between healthy and glaucoma images.

Figure 5.2 showed the low performance of the features that extracted from un-preprocessing images using the features of the two extracted methods alone and even when the extracted features of the two extracted methods in RIM-ONE (V1) database were combined.

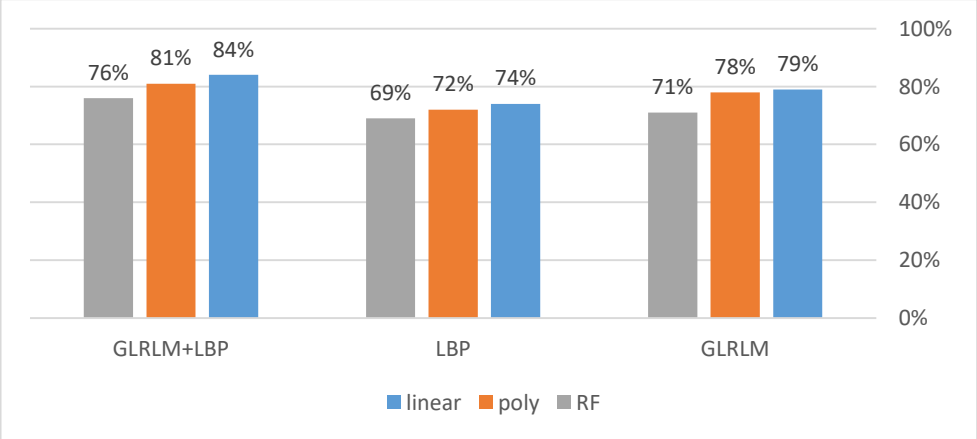

Figure 5.2: The accuracy results of RIM-ONE (V1) using First Experiment.

Almost the specificity metric had high values where the sensitivity had low values, where most glaucoma images were missed classified may due to the imbalance data in V1 of RIM-ONE that contained 51 glaucoma images where healthy images are 118.

In V2 of RIM-ONE database, the accuracy values of GLRLM features was more accurate than LBP histogram features with Ten-fold cross-validation as presented in Table 5.2. However, after combined the features the result values were improved and reached to 82% where the highest accuracy with linear SVM classifier but also the results were not promising. The performance of linear SVM classifier was the highest compared to polynomial SVM and RF also the results of the V2 of RIM-ONE were less compared to the performance of V1 of the database.

Table 5.2: The results of RIM-ONE (V2) database using SVM and RF classifiers in First Experiment.

Feature Extraction Method	Classifier	Kernel	Specificity	Sensitivity	Accuracy	Cross-validation Accuracy
GLRLM	SVM	Linear	68%	81%	75%	80%
		Polynomial	38%	95%	69%	72%
	RF		69%	77%	73%	70%
LBP	SVM	Linear	66%	79%	73%	76%
		Polynomial	33%	90%	64%	68%
	RF		61%	71%	67%	67%
LBP + GLRLM	SVM	Linear	69%	85%	78%	82%
		Polynomial	41%	93%	69%	74%
	RF		63%	83%	74%	75%

The accuracy values were improved with small ratio when the extracted features of the LBP and GLRLM methods were combined in one vector as showed in Figure 5.3.

Table 5.3 presented the results of V3 of database, as in V1 and V2 of RIM-ONE database the performance of statistical features of LBP descriptor were less than the GLRLM features performance with the three classifier, features combination increased the performance especially with RF classifier with 70%, while linear SVM classifier achieved the high accuracy with Ten-fold cross-validation was 74%.

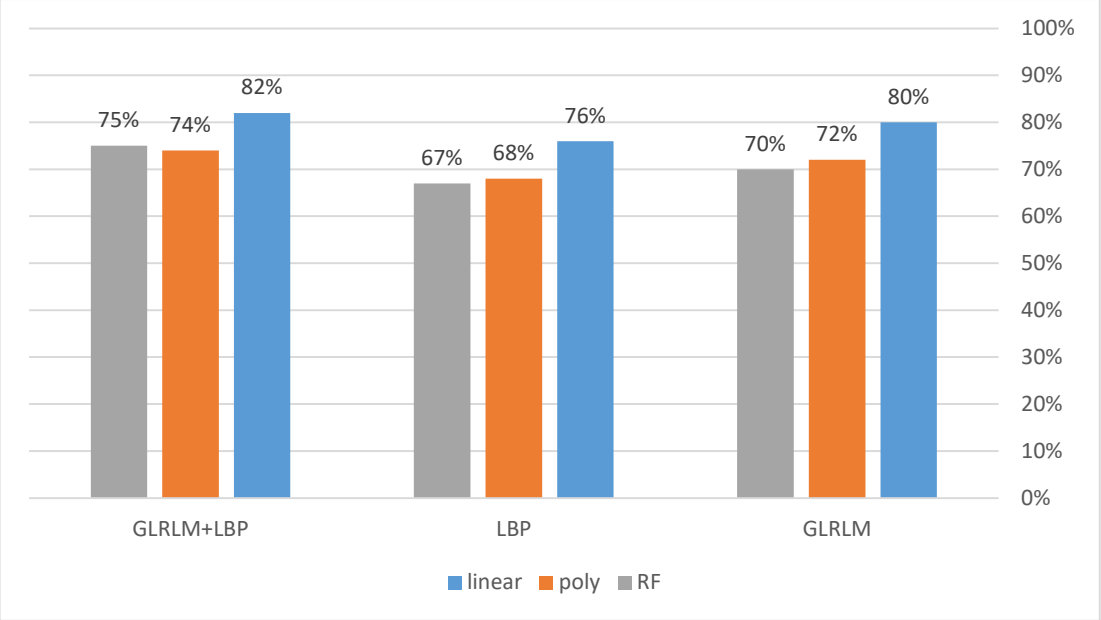

Figure 5.3: The accuracy results of RIM-ONE (V2) using First Experiment.

Table 5.3: The results of RIM-ONE (V3) database using SVM and RF classifiers in First Experiment.

Feature Extraction Method	Classifier	Kernel	Specificity	Sensitivity	Accuracy	Cross-validation Accuracy
GLRLM	SVM	Linear	78%	58%	66%	70%
		Polynomial	94%	73%	60%	72%
	RF		73%	41%	54%	66%
LBP	SVM	Linear	89%	62%	72%	64%
		Polynomial	47%	93%	75%	63%
	RF		47%	51%	50%	51%
LBP + GLRLM	SVM	Linear	78%	62%	68%	74%
		Polynomial	94%	31%	56%	73%
	RF		84%	65%	72%	70%

Figure 5.4 showed the low performance of RIM-ONE V3 database compared to V1 and V2, where the accuracy values of extracted features were the lowest compared to other versions of database, that may due to the small set of glaucoma and healthy

images and the resizing process where the images in V3 have high resolution with size of (2144x1424) and resized to (512x512) that may occur losing lots of image data.

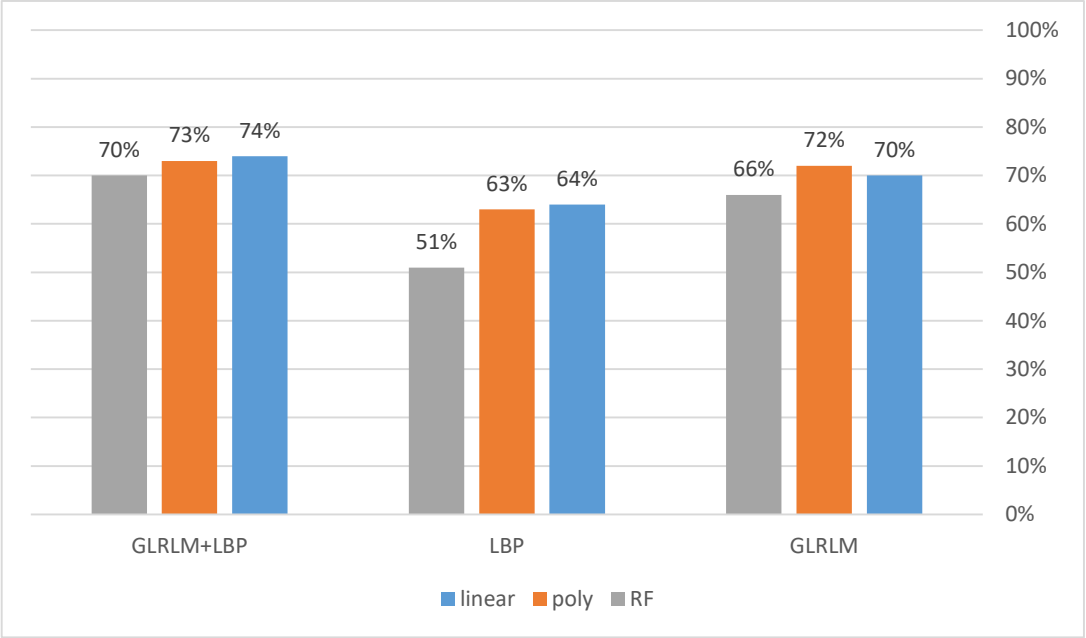

Figure 5.4: The accuracy results of RIM-ONE (V3) using First Experiment.

The high values of specificity and the low in sensitivity values in V1 of the database using SVM classifiers refer to the model classified all images as non-glaucoma that may due to the large number of non-glaucoma images compared to glaucoma images. Although the data balanced in RIM-ONE V2 and V3, but the accuracy values were not improved compared to V1 of RIM-ONE.

Form the first experiment, GLRLM features had higher performance than LBP histogram features depending on the results of the three versions of database and classifiers. In addition, linear SVM classifier had the best results compared to polynomial SVM and RF classifiers.

5.2 Second Experiment: Combination of LBP and GLRLM with Preprocessing:

The second experiment was similar to the previous one with one difference that the preprocessing method was applied in experiment 2 as in Figure 5.5. Eliminate the noise, artifact, and enhancement the image played critical role in CAD systems and in classification performance.

The two different between the second experiment and proposed methodology in Figure 4.1 were in preprocessing and feature extraction stages. Firstly, in experiment 2, the

color image was separated to R-G-B planes that inputted in preprocessing method and feature extraction methods.

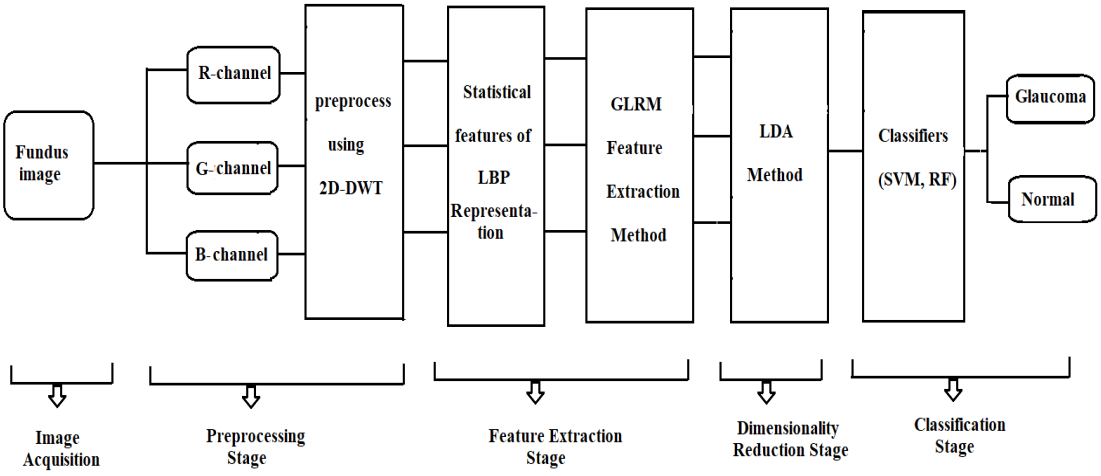

Figure 5.5: The methodology of Combination of LBP and GLRLM with preprocessing.

The second difference in second experiment was extracted seven statistical features of LBP representation.

In the second experiment, 2D-DWT method was performed to de-noising database images to increase pattern recognition and obtain more accurate features using feature extraction methods. Where each image separated to R-G-B channels after resizing all images to 512x512. The extracted channels were de-noising using 2D-DWT that eliminated the noise and artifacts of database images. The features were extracted using LBP descriptor and GLRLM that applied on each component in an image.

The effect of the preprocessing method was evaluated by comparing the results of extracted features of LBP and GLRLM methods, where each method alone, then the features of the two methods were combined to evaluate the performance of the results using SVM and RF classifiers.

The features vector of each image was the combination of features vector of each component that mean the features vector length of GLRLM for each image was forty eight features with sixteen features for each component. In LBP feature vector, also it consisted of twenty one features, which the combination of seven features of each component of an image.

In the features combination of GLRLM and LBP, seven histogram features and sixteen GLRLM features were extracted from each image component, the extracted features of R-G-B components were combined in sixty nine vector length for each image.

LDA discriminant method applied min-max normalization on feature vectors of the two extracted methods and to the combination of extracted feature, then produce three discriminant vectors that used to train the classifiers.

The results of RIM-ONE V1 database showed in Table 5.4, sufficient improvement was noted in the performance results comparing to first experiment with applying 2D-DWT and used separation images. The performance of GLRLM features also more accurate than statistical features of LBP descriptor, where the accuracy values with 10 fold cross-validation of GLRLM features were 89% where with statistical LBP descriptor was 81% with linear SVM.

Table 5.4: The results of RIM-ONE (V1) database using SVM and RF classifiers in Second Experiment.

Feature Extraction Method	Classifier	Kernel	Specificity	Sensitivity	Accuracy	Cross-validation Accuracy
GLRLM	SVM	Linear	81%	94%	90%	89%
		Polynomial	81%	97%	92%	89%
	RF		62%	91%	82%	85%
LBP	SVM	Linear	50%	88%	76%	81%
		Polynomial	37%	100%	80%	81%
	RF		56%	80%	72%	69%
LBP + GLRLM	SVM	Linear	93%	100%	98%	96%
		Polynomial	93%	100%	98%	95%
	RF		100%	94%	96%	95%

The magnificent improvement in classifiers performance was obtained after perform combination features of LBP and GLRLM methods, the accuracy values were improved as in Figure 5.6, where accuracy achieved to 96% with linear SVM classifier and 95% with polynomial and RF classifiers.

As in V1, the V2 of database had better performance values of classifiers after obtaining features from de-noising images, the classifiers performance that used

GLRLM features were higher than that obtained from experiment 1. Where the classifiers that trained with histogram features of LBP obtained lower values as showed in Figure 5.7, but also higher than the results values of the first experiment.

The accuracy values of the features combination vector of the two extracted methods had high accuracy values as presented in Table 5.5, compared to combination features of un-preprocessed images in first experiment. Where the highest performance values of classifiers reached to 87% with linear SVM.

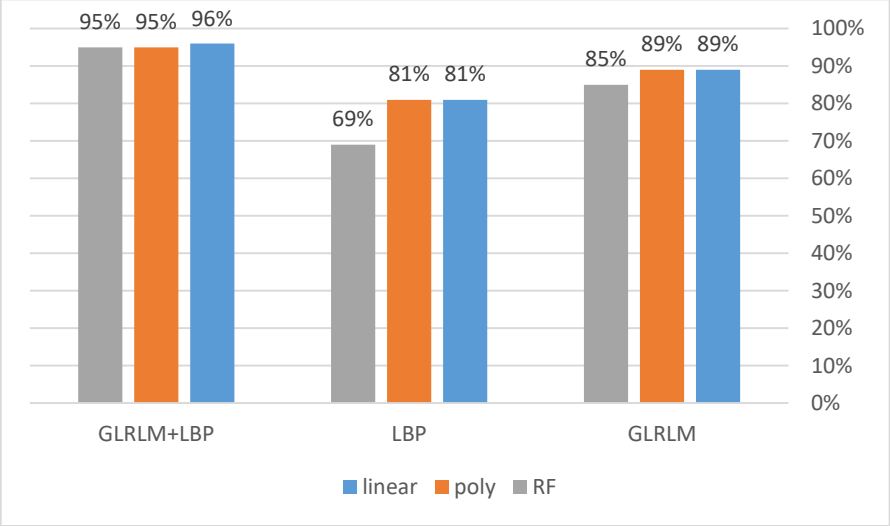

Figure 5.6: The accuracy results of RIM-ONE (V1) using Second Experiment.

Table 5.5: The results of RIM-ONE (V2) database using SVM and RF classifiers in Second Experiment.

Feature Extraction Method	Classifier	Kernel	Specificity	Sensitivity	Accuracy	Cross-validation Accuracy
GLRLM	SVM	Linear	79%	83%	81%	83%
		Polynomial	57%	97%	78%	81%
	RF		73%	67%	70%	75%
LBP	SVM	Linear	69%	77%	73%	77%
		Polynomial	49%	93%	72%	74%
	RF		65%	71%	68%	67%
LBP + GLRLM	SVM	Linear	87%	83%	85%	87%
		Polynomial	73%	94%	84%	84%
	RF		95%	86%	90%	83%

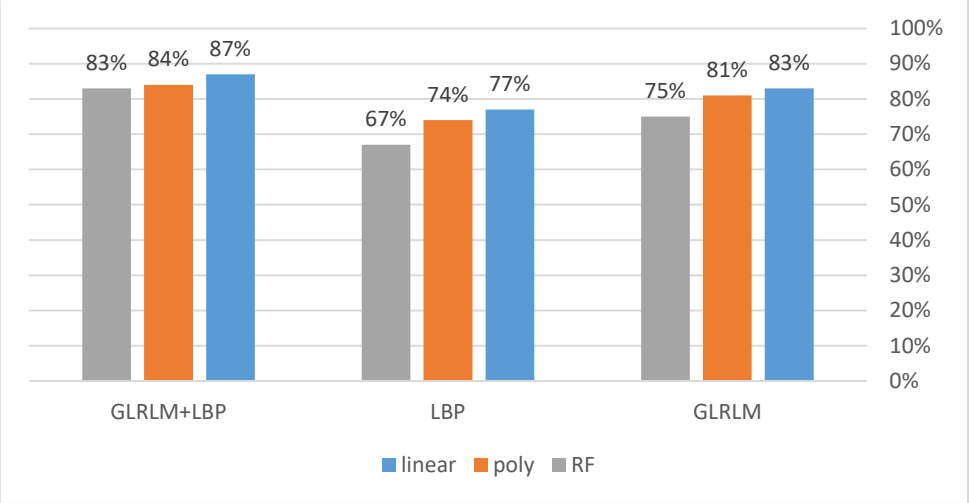

Figure 5.7: The accuracy results of RIM-ONE (V2) using Second Experiment.

Such as V1 and V2 of RIM-ONE database, the accuracy values of RIM-ONE V3 were improved when the images were preprocessed and used separation channels of the images as presented in Table 5.6. The results of GLRLM features had more accurate performance compared to LBP features. While the performance improved when the features of the two methods were combined to 87% with linear SVM with ten-fold cross-validation. As plotted in Figure 5.8, SVM classifier that used linear kernel function had the highest performance compared to the polynomial SVM and RF classifiers with all feature vectors that used to train a model.

Table 5.6: The results of RIM-ONE (V3) database using SVM and RF classifiers in Second Experiment.

Feature Extraction Method	Classifier	Kernel	Specificity	Sensitivity	Accuracy	Cross-validation Accuracy
GLRLM	SVM	Linear	73%	75%	75%	78%
		Polynomial	52%	89%	75%	75%
	RF		89%	55%	68%	71%
LBP	SVM	Linear	84%	68%	75%	69%
		Polynomial	42%	89%	70%	60%
	RF		73%	62%	66%	59%
LBP + GLRLM	SVM	Linear	94%	86%	89%	87%
		Polynomial	89%	100%	95%	88%
	RF		89%	82%	85%	83%

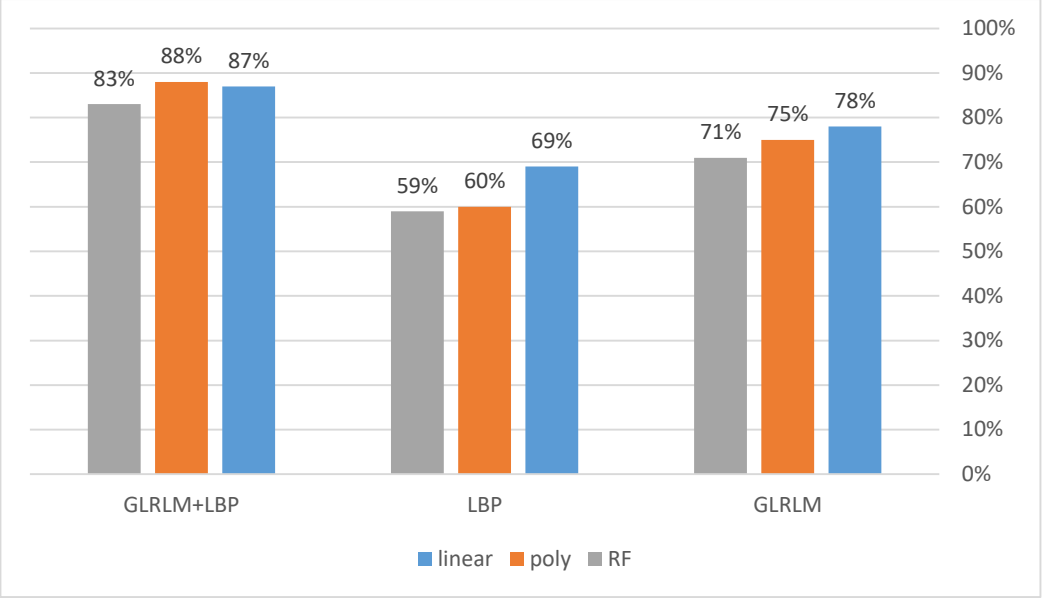

Figure 5.8: The accuracy results of RIM-ONE (V3) using Second Experiment.

5.3 Third Experiment: Conjunction of LBP and GLRLM:

The proposed methodology that showed in Figure 4.1 was implemented in the third experiment, where all stages of CAD was performed except segmentation due to this research extracted non-structured features. The main contributions in third experiment were obtained four images (R-G-B components and grayscale images) from each input image that performed preprocessing method on them and used in feature extraction stages.

The second contribution was applied GLRLM method on binary LBP representation directly to extract GLRLM features instead of extract statistical histogram features. That mean the common statistical features were dispensed and just was used the features that evaluate the spatial distribution of gray level values.

In this experiment, after applying 2D-DWT as a de-noising method to preprocessing the images, usually LBP descriptor was used to convert the image to binary image (LBP representation) as in Figure 4.5 followed by extracted statistical features from LBP histogram such as experiments 1 and 2.

This work aimed to present the powerful of extracted feature methods combination with different aspects, instead of extract statistical histogram features of LBP representation as in experiment 2, GLRLM method was applied directly on LBP

representation to obtain different gray level distribution features and compared the results with experiment 2 that applied traditional concept of extract LBP features.

In addition, of applied 2D-DWT on R-G-B separated channels, the grayscale image was added, which mean four images were used to represent on image. Where each image used to extract sixteen GLRLM features that mean the vector length of the four R-G-B and grayscale images was sixty four features.

The performance of the features of each component alone was computed, followed by combined in R-G-B vector with 48 features. Finally, combine all the 64 features in one vector to train the three classifiers after applying LDA to reduce the dimensionality.

Results of V1 of RIM-ONE database using sensitivity, specificity, accuracy, and 10-fold cross-validation accuracy were presented in Table 5.7.

The results of 10-fold cross validation observed that green channel images obtained the lowest results using the two classifiers compared to red and blue channels that had better results than G component and grayscale images. Where the red component images obtained the highest values of accuracy compared to other separated channels and grayscale images.

When the features of RGB component were combined in one vector, the performance of classifiers improved compared to use extracted features of each component alone. Where the accuracy developed to 94% using polynomial SVM classifier.

The sufficient improvement occurred when GLRLM features of RGB channels were combined with grayscale image as presented in Figure 5.9, where the performance of the classifiers was developed and the accuracy value reached 97% using linear SVM classifier.

The specificity values reached 100% with RGB features and the features combination of RGB and grayscale images, where the high value of specificity means all healthy images are classified correctly that implied the model learned well with large number of non-glaucoma images compared to disease cases in V1 of RIM-ONE database.

The results of classifiers performance that applied on version 2 (V2) of RIM-ONE database are listed in Table 5.8.

Table 5.7: The results of RIM-ONE (V1) database using SVM and RF classifiers in Third Experiment.

Image	Classifier	Parameters	Sensitivity	Specificity	Accuracy	Cross-Validation Accuracy
Grayscale	SVM	Linear	43%	97%	80%	79%
		Polynomial	31%	100%	78%	77%
	RF		68%	88%	82%	74%
R	SVM	Linear	68%	100%	90%	82%
		Polynomial	37%	100%	80%	79%
	RF		62%	80%	74%	70%
G	SVM	Linear	25%	100%	76%	77%
		Polynomial	25%	100%	76%	74%
	RF		37%	80%	66%	67%
B	SVM	Linear	50%	88%	76%	80%
		Polynomial	25%	100%	76%	76%
	RF		56%	74%	68%	67%
RGB	SVM	Linear	87%	100%	96%	92%
		Polynomial	87%	100%	96%	94%
	RF		81%	100%	94%	87%
R-G-B, Grayscale	SVM	Linear	93%	100%	**98%**	**97%**
		Polynomial	93%	100%	**98%**	95%
	RF		87%	100%	96%	94%

In opposite of V1 of the database results, red component obtained the lowest results compared to green, blue and grayscale images, where the grayscale images features had the highest results with 78% with linear SVM compared to the results of each component alone as plotted in Figure 5.10.

Such as V1 of database, the accuracy results were developed when the extracted features of RGB component were combined in one vector to train the classifiers, where the accuracy result reached to 86% with linear SVM. The highest accuracy value of V2 achieved resulting of combine the features of RGB component with grayscale features, where the performance of linear SVM increased to 89%.

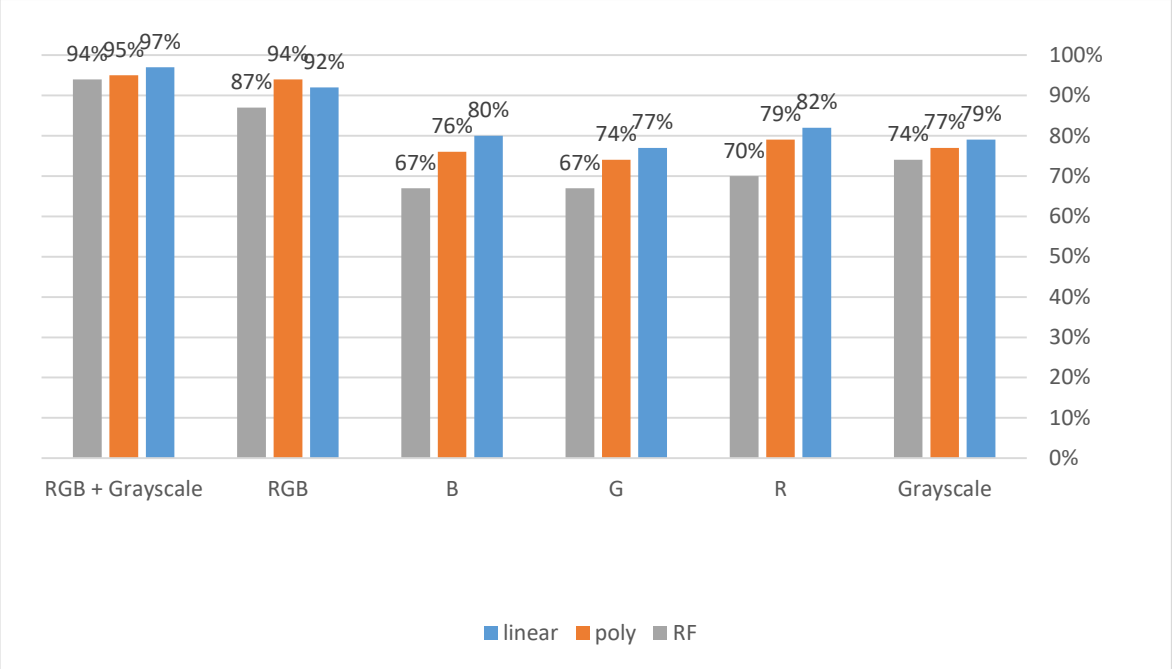

Figure 5.9: The accuracy results of RIM-ONE (V1) using Third Experiment.

Table 5.9 observed the results of accuracy metrics of classifiers performance that trained using V3 of RIM-ONE database. Such as V1, green channel had the lowest accuracy results, where blue channel obtained the highest results compared to other separated channels and grayscale images. As in V1 and V2 versions of database, the classifiers performance improved after combine RGB components features in one vector, where the accuracy values improved to 86% with linear SVM.

In addition, the results become more accurately after combine grayscale features to the feature vector of RGB components as plotted in Figure 5.11, where the accuracy developed to 95% with polynomial SVM classifier.

The extracted features of R-G-B channels or grayscale images separately could not describe glaucoma pattern, where all previous accuracies have low values, due to the classifiers do not obtain meaningful features when each plane was processed alone than when the features of RGB components were concatenated.

When grayscale image was used with RGB components of images, the highest accuracies were achieved compared to the previous results. In V1, V2, and V3 of RIM-ONE database, the highest accuracies achieved when RGB features vectors were concatenated with grayscale features that extracted from LBP representations and GLRLM method.

Table 5.8: The results of RIM-ONE (V2) database using SVM and RF classifiers in Third Experiment.

Image	Classifier	Parameters	Sensitivity	Specificity	Accuracy	Cross-Validation Accuracy
Grayscale	SVM	Linear	69%	81%	75%	78%
		Polynomial	41%	94%	70%	70%
	RF		63%	71%	67%	65%
R	SVM	Linear	63%	78%	71%	69%
		Polynomial	30%	91%	63%	65%
	RF		58%	59%	56%	62%
G	SVM	Linear	58%	81%	70%	74%
		Polynomial	36%	64%	67%	70%
	RF		63%	71%	67%	64%
B	SVM	Linear	65%	79%	72%	77%
		Polynomial	33%	94%	66%	70%
	RF		57%	68%	63%	67%
R-G-B	SVM	Linear	88%	85%	86%	86%
		Polynomial	69%	74%	83%	81%
	RF		74%	81%	78%	80%
R-G-B, Grayscale	SVM	Linear	90%	93%	**91**%	**89**%
		Polynomial	73%	95%	85%	83%
	RF		90%	82%	86%	85%

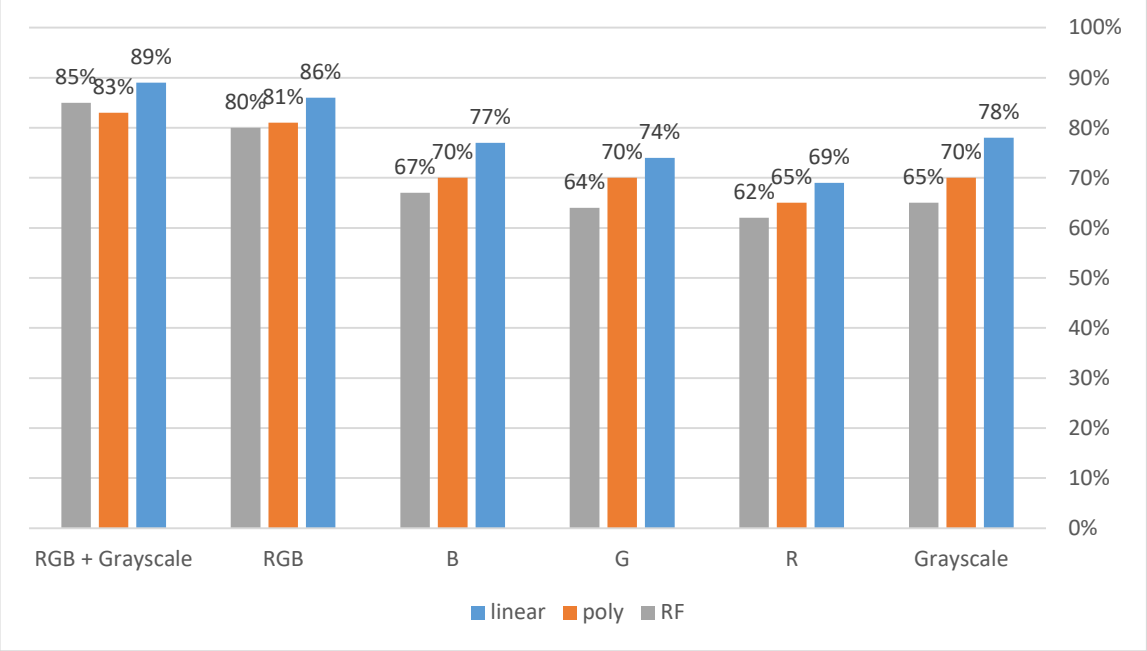

Figure 5.10: The accuracy results of RIM-ONE (V2) using Third Experiment.

Table 5.9: The results of RIM-ONE (V3) database using SVM and RF classifiers in Third Experiment.

Image	Classifier	Parameters	Sensitivity	Specificity	Accuracy	Cross-Validation Accuracy
Grayscale	SVM	Linear	52%	79%	68%	69%
		Polynomial	52%	100%	62%	59%
	RF		73%	62%	66%	63%
R	SVM	Linear	63%	72%	68%	69%
		Polynomial	56%	56%	62%	69%
	RF		63%	55%	58%	60%
G	SVM	Linear	78%	79%	79%	67%
		Polynomial	58%	93%	77%	63%
	RF		78%	55%	64%	67%
B	SVM	Linear	73%	86%	81%	71%
		Polynomial	36%	100%	75%	64%
	RF		73%	55%	62%	59%
R-G-B	SVM	Linear	89%	89%	89%	86%
		Polynomial	84%	96%	91%	83%
	RF		84%	93%	89%	80%
R-G-B, Grayscale	SVM	Linear	100%	96%	**97**%	89%
		Polynomial	89%	96%	93%	**95**%
	RF		94%	93%	93%	86%

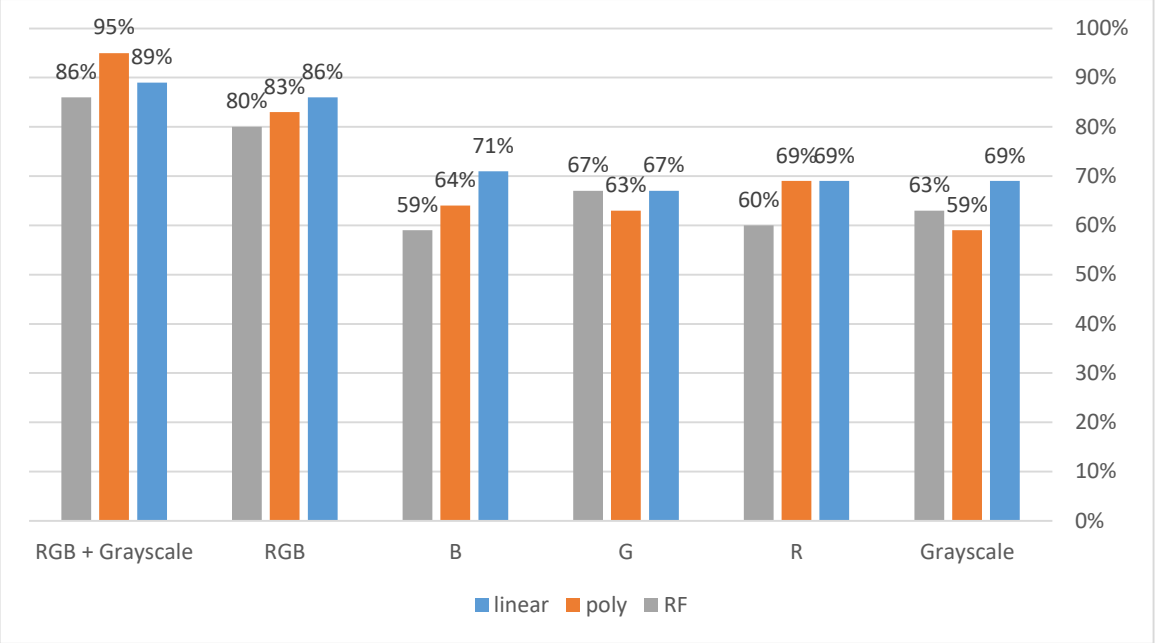

Figure 5.11: The accuracy results of RIM-ONE (V3) using Third Experiment.

The results of linear SVM had higher performance than polynomial SVM classifier in V1 and V2 database versions. Wherein V3 images, the polynomial classifier was the highest performance, where RF classifier had the lowest accuracy performance compared to linear and polynomial SVM classifiers when they learned using extracted features.

Although many researchers used grayscale images in their methodologies (Shinde, 2021) (Thakur & Juneja, 2020) (Claro et al., 2019) (Krishnamoorthi & Chinnababu, 2019) or used R-G-B channels to detect glaucoma (Khan et al., 2021), this research obtained the best results when the grayscale image and image components were combined.

From experiments 1 and 2, this work concluded the important contribution of preprocessing stage and how it improved the obtaining of effective features and accurate results. Combining the features in experiments 1 and 2 or combining feature extraction methods as in experiment 3 contributed to improve the classifiers performance.

In experiment 1 and 2, GLRLM features had performance more accurate than LBP histogram features, although LBP descriptor was used extensively in glaucoma detection, and rarely applied GLRLM method. In addition, linear SVM classifier had the best results in all experiments compared to polynomial SVM and RF classifiers.

From experiment 3, it concluded that a combination set of texture features improved the accuracy compared to dealing with each image component as an independent unit. Although many researchers commonly used grayscale images in their glaucoma detection studies, the image channels could provide more information for glaucoma identification. Linear SVM classifier had the highest performance compared to polynomial and RF classifier when they carried out on R-G-B and grayscale feature vector.

5.4 Misclassified Images of Conjunction of LBP and GLRLM

Twenty five images of the 783 images of RIM-ONE database were classified incorrectly using the conjunction on LBP and GLRLM. The number of correct and incorrect classified images of RIM-ONE database versions was listed in Table 5.10.

Table 5.10: The number of correct and misclassified images in versions of RIM-ONE database in our Methodology.

Classified	RIM-ONE V1		RIM-ONE V2		RIM-ONE V3		Total no. Images
	Glaucoma	Healthy	Glaucoma	Healthy	Glaucoma	Healthy	
Incorrect	2	0	7	11	2	3	25
Correct	49	118	193	244	72	82	783

5.4.1 Misclassified Images of RIM-ONE Version 1:

Two images of V1 of database were classified incorrectly with linear SVM model that trained using combination of RGB and grayscale features of GLRLM method that extracted from LBP representation. In Figure 5.12, the two images were glaucoma and classified as healthy images, the left image was moderate glaucoma case, where the right image was early glaucoma severity. Twelve glaucoma images of RIM-ONE (V1) were categorized as early glaucoma cases that mean they were difficult to detection also for specialist and our model misclassified just one of them that observed the efficiency of our model.

5.4.2 Misclassified Data of RIM-ONE Version 2:

Linear SVM classifier misclassified seven glaucoma images and eleven healthy images in V2 of RIM-ONE database in experiment 3. The left image in Figure 5.13 was glaucoma image, where the right image was healthy image that classified incorrectly from RIM-ONE (V2) database.

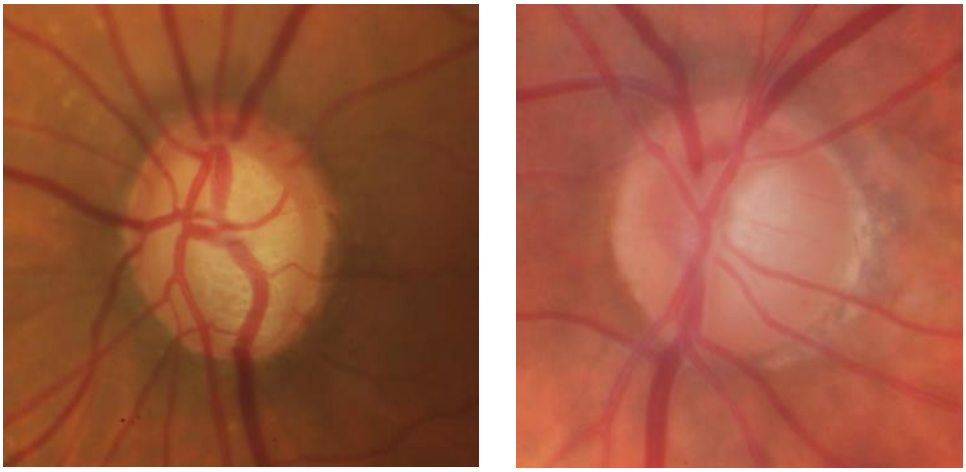

Figure 5.12: Misclassified images in V1 of RIM-ONE database.

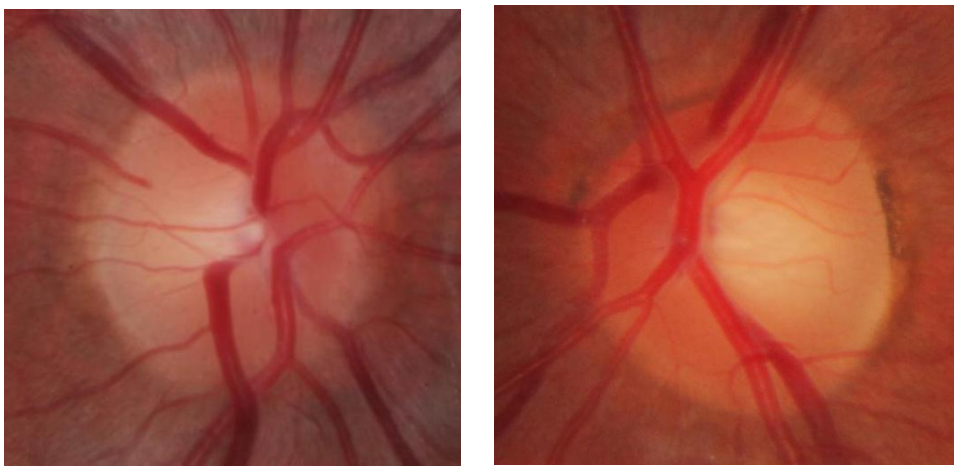

Figure 5.13: Misclassified images in V2 of RIM-ONE database.

5.4.3 Misclassified Data of RIM-ONE Version 3:

Five images misclassified from the third version of database with linear SVM classifier of experiment 3. Two images were glaucoma and the else were healthy images. The Figure 5.14 observed the glaucoma image in the left side and in the right side was the healthy image, from that images it observed the difficulty of detect glaucoma features from that dark images.

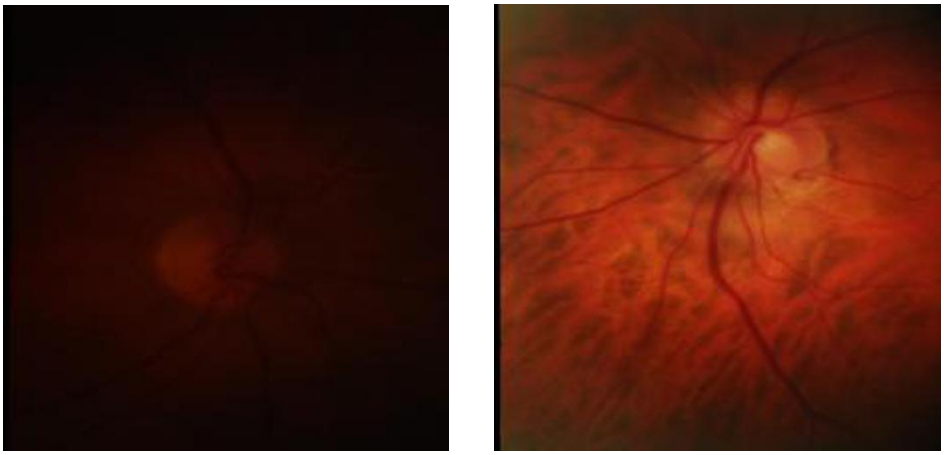

Figure 5.14: Misclassified images in V3 of RIM-ONE database.

5.5 Evaluate The Misclassified Images Using Ophthalmology Experts

Our methodology achieved high results, but it had ratio of misclassification. The researcher tried to evaluate the misclassified data by classify them by ophthalmology experts to observe the efficiency of our technique compared to their results.

Four ophthalmology experts contributed in our research, first expert was Head of Ophthalmology Department (HOD) Faculty of Medicine- University Of Benghazi and interest with glaucoma disease, when she screened the existing of glaucoma in twenty five images that misclassified, first expert diagnosed the images such as listed in Table 5.11. Each image was classified as glaucoma, healthy or not clear image and need to more measurements to confirm the screening.

Table 5.11: The results of First ophthalmology Expert diagnosis of misclassified images in Versions of RIM-ONE database.

	RIM-ONE V1	RIM-ONE V2		RIM-ONE V3		Accuracy of Diagnosis
	Glaucoma	Glaucoma	Healthy	Glaucoma	Healthy	
Correct classification	1	1	0	0	1	12%
Incorrect classification	0	0	3	0	2	20%
Not Clear	1	6	8	2	0	68%

First expert classified just two images correctly, where one was glaucoma image and the other was healthy image. Five images were classified incorrectly and eighteen images were mentioned as not clear for diagnosis and need to more tests.

Second expert was Tunisian ophthalmologist professor that scanned the fundus photographs and reported the diagnosis of glaucoma as listed in Table 5.12. Fourteen fundus images were classified correctly by the second expert, where five of them were glaucoma images and the nine were healthy images. Seven images were misclassified and four fundus images were mentioned as not cleared.

Table 5.12: The results of Second ophthalmology Expert diagnosis of misclassified images in versions of RIM-ONE database.

	RIM-ONE V1	RIM-ONE V2		RIM-ONE V3		Accuracy of Diagnosis
	Glaucoma	Glaucoma	Healthy	Glaucoma	Healthy	
Correct classification	2	3	7	0	2	56%
Incorrect classification	0	3	3	1	0	28%
Not Clear	0	1	1	1	1	16%

The third expert was associate professor and Head of Ophthalmic Department (HOD) in Omar Al-Mukhtar University, the expert classified the twenty five images as showed in Table 5.13. The glaucoma was detected in five images correctly of eleven glaucoma fundus images. Eleven fundus photographs were classified correctly as healthy images of fourteen fundus images, where four images were stated as unclear to diagnosis.

Table 5.13: The results of Third ophthalmology Expert diagnosis of misclassified images in versions of RIM-ONE database.

	RIM-ONE V1	RIM-ONE V2		RIM-ONE V3		Accuracy of Diagnosis
	Glaucoma	Glaucoma	Healthy	Glaucoma	Healthy	
Correct classification	1	4	9	0	2	64%
Incorrect classification	1	2	1	1	0	20%
Not Clear	0	1	1	1	1	16%

The fourth expert was senior registrar Ophthalmologist, detecting the existing of glaucoma correctly in three images of eleven glaucoma fundus image, where the healthy images that classified correctly by the fourth expert were eleven images of

fourteen healthy fundus images. One image stated as unclear for diagnosis. The results of fourth expert diagnosis listed in Table 5.14.

Table 5.14: The results of Fourth ophthalmology Expert diagnosis of misclassified images in versions of RIM-ONE database.

	RIM-ONE V1	RIM-ONE V2		RIM-ONE V3		Accuracy of Diagnosis
	Glaucoma	Glaucoma	Healthy	Glaucoma	Healthy	
Correct classification	1	2	8	0	3	56%
Incorrect classification	1	5	3	1	0	40%
Not Clear	0	0	0	1	0	4%

The accuracy of correct diagnosis of the first expert was 12%, where the diagnosis accuracy of the second and fourth experts was 56%, the best performance was obtained by the third expert with 64%. Where the ration of unclear images of the first expert was 72%, and 16% for the second and third expert. Fourth expert mentioned one image as not cleared with ratio 4%.

The accuracy performance of experts was good as almost 50% of the misdiagnosed images that mentioned as not cleared or had other diseases. In addition, many images were diagnosed as glaucoma suspect that experts need to more measurements to ensure the diagnosis.

Figure 5.15 showed some images that misclassified images from all experts. In image, (a) one expert stated that titling the disc face make unclear lower edge of the optic disc and mentioned as not clear, where the other experts reported the image was healthy.

The (b) and (c) images were diagnosed by all experts as normal while the images was glaucoma as classified in RIM-ONE database (V2). The experts mentioned that CDR and rim area were normal in both images, although the images were glaucoma.

The experts mentioned that image (d) had unclear lower edge of the optic disc and needed to calculate other parameters as Retinal Nerve Fiber Layer, Peripapillary Chorioretinal Atrophy, Lamina cribrosa and others.

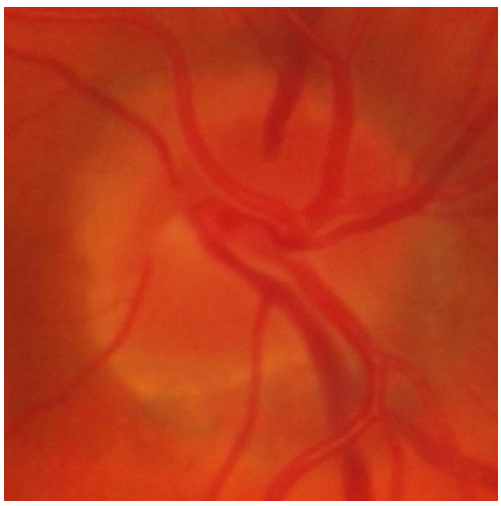

(a) Not clear

(b) Misclassified

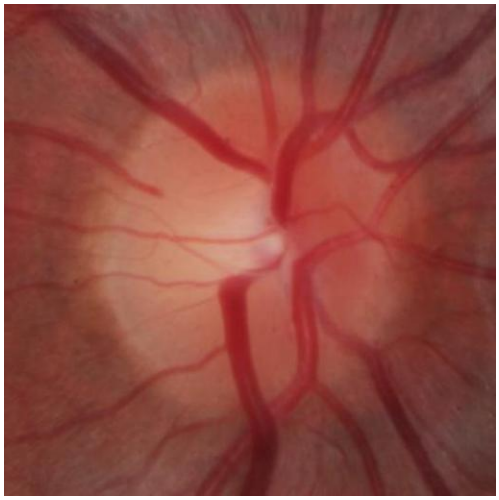

(c) Misclassified

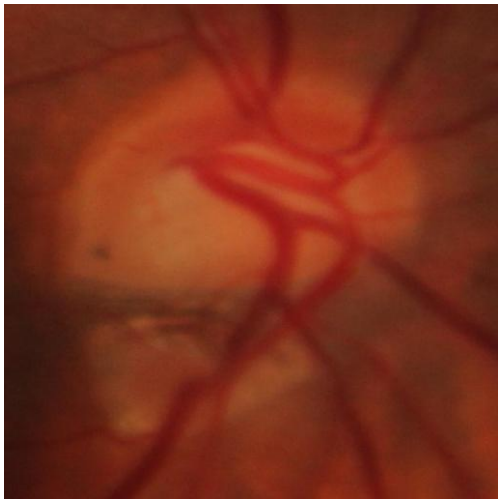

(d) Not clear lower edge

(e) Unclear cup

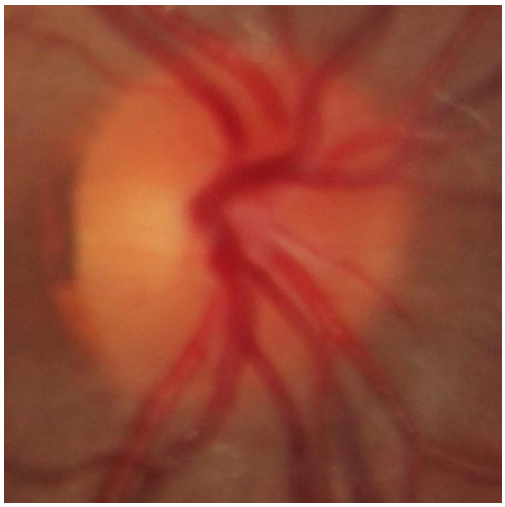

(f) Obliterated cup

Figure 5.15: The images that misclassified images from all experts.

The five image (e) was mentioned by one expert as not clear cup, other experts diagnosed the image as normal, although the image was glaucoma.

The image (f) had obliterated cup but not had glaucoma changes as expert stated, due to that the image classified as normal while the image was glaucoma. Other expert mentioned that the image (f) had other eye disease (myopia).

Other measurements were critical factors for ophthalmologist to detect the glaucoma in fundus images, many ophthalmologists that the researcher contacted with them, they mentioned that they used other medical measurement with fundus images to screening the glaucoma such as visual field and intraocular pressure measurement, they stated they had no ability to detect glaucoma using fundus images alone.

5.6 Comparing the Results with Other Related Literature

Many approaches were proposed for glaucoma diagnosis, often they used common methods to analyze image texture, and some of them had used Deep Learning techniques. The same classifier and database with different versions were used in our proposed and in related works. The results of previous studies, feature extraction methods, and classifiers showed in Table 5.12.

The results of the proposed method were promising compared to current literature. With same classifier and database version, khan *et al.* (Khan et al., 2021), shinde (Shinde, 2021) and Thakur and Juneja (Thakur & Juneja, 2020) were inline with us also in the same homogenous size of database images. In (Shinde, 2021), morphological features were used to train the model, but the proposed study proved that non-morphological features could obtain high results. Although, Carlo *et al*. (Claro et al., 2019) used a common method to extract statistical features (Grey level co-occurrence matrix) (GLCM) and used seven CNN architectures to obtain features that were not visible for the human eye, without preprocessing the grayscale image, which could limit the performance of the approach. Krishnamoorthi and Chinnababu (Krishnamoorthi & Chinnababu, 2019) and Chaudhary and Pachori (Chaudhary & Pachori, 2021) used various feature extraction methods on grayscale images with the same classifier. Although (Thakur & Juneja, 2020) used structured and non-structured features to train SVM, however, using channel separation and spatial features contributed to obtaining better results in our work and without the need for optic disc segmentation as in De Sousa *et al.* (de Sousa et al., 2017). This research performed the

de-noising method as in (Khan et al., 2021). R-G-B channels were preprocessed and used to extract statistical features in (Khan et al., 2021), this work suggested using a grayscale image with R-G-B channels of an image and that contributed to capturing more detailed information about glaucoma images and contributed to increasing the performance of the classifiers.

Table 5.12: Comparison the results of our Methodology with related works.

Author	Extracted Features	Classifier	RIM-ONE Version	Accuracy
Shinde (Shinde, 2021)	CDR + ISNT + blood vessel ratio	Voting (SVM, NN and Adaboost)	V1	96%
Carlo *et al.* (Claro et al., 2019)	GLCM + CNNs	SVM, MLP, RF	V1	93%
Krishnamoorthi and Chinnababu (Krishnamoorthi & Chinnababu, 2019)	LBP + HOG + Fractal features	SVM	V1	91%
Chaudhary and Pachori (Chaudhary & Pachori, 2021)	GLCM + Chip features + invariant moment features	SVM	V1 V2	90% 90%
De Sousa *et al.* (de Sousa et al., 2017)	LBP + Geostatistical features	SVM	V2	90%
Thakur and Juneja (Thakur & Juneja, 2020)	Structural and Non-structural features	SVM	V3	93%
khan *et al.* (Khan et al., 2021)	Statistical features	LS-SVM	V3	91%
Proposed Methodology	LBP representations + GLRLM	SVM	V1 V2 V3	98% 91% 97%

The proposed method improved the state-of-the-art glaucoma diagnosis results. The results demonstrated the extracted GLRLM features from LBP-represented images had better performance compared to extracted statistical features from (Krishnamoorthi & Chinnababu, 2019) (Claro et al., 2019) and (Srinivasan et al., 2016).

5.7 Summary

Preprocessing phase had a critical role in CAD system and in pattern recognition. Separate the image to channels provided more information about texture in an image

compared to use grayscale image alone. The performance of classifiers in second experiment improved significantly compared to first experiment results. In the experiments 1 and 2, the results of GLRLM features were more accurate than LBP histogram features, although LBP descriptor was applied widely in glaucoma detection area but it given less accuracy results than GLRLM that rarely applied in the research domain.

When the results of the three experiments were compared, that observed that experiment 1 had the lowest performance results compared to experiments 2 and 3 that due to many factor. Firstly, the original images were used without applying preprocessing method to enhance the images and remove the noise. Secondly, the grayscale image was used alone to detect pattern and extract the features from an image.

The results of experiment 2 was closed to experiment 3 results, although extract GLRLM features from LBP representation (experiment 3) had the best results. In the third experiment, the linear SVM classifier when training on GLRLM features of R-G-B and grayscale images had the best results of glaucoma detection in all versions of RIM-ONE database as shown in Figure 5.16, Figure 5.17 and Figure 5.18 that presented the performance of RIM-ONE V1, V2 and V3 in the three experiments respectively.

It can be concluded that a combination set of texture features had improved the accuracy compared to dealing with each component as an independent unit. Although many researchers commonly used grayscale images in their glaucoma detection studies, the image channels could provide more information for glaucoma identification.

Although the robustness of RF classifier against overfitting, but it had the lowest performance compared to SVM classifiers, where linear SVM classifier had more accurate results in experiments 1, 2 and 3.

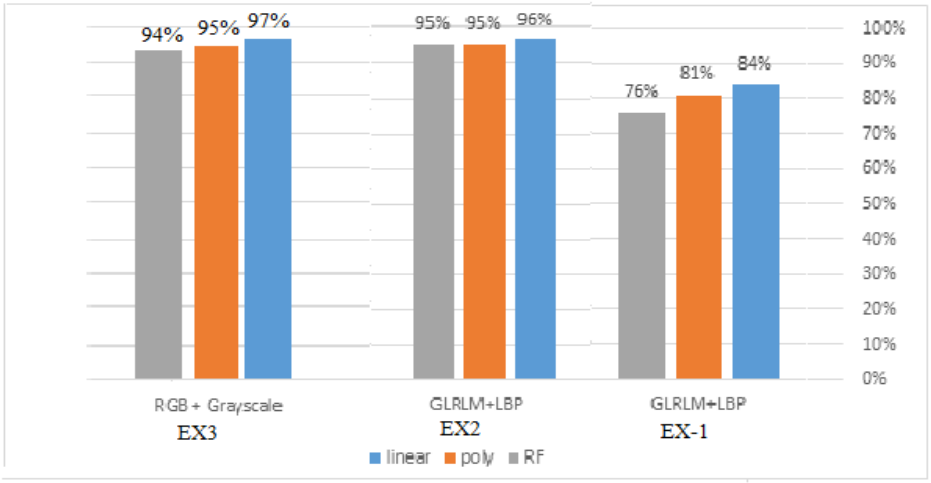

Figure 5.16: Comparing the performance of the three Experiments using RIM-ONE (V1) database.

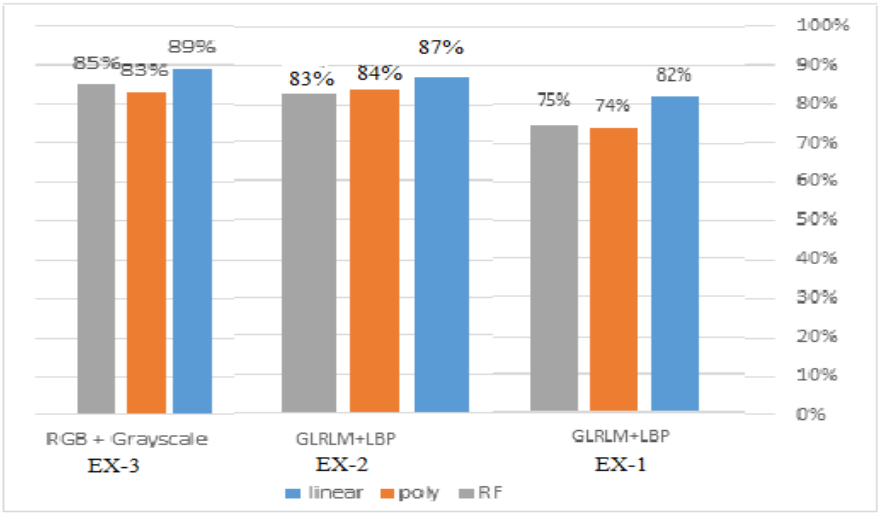

Figure 5.17: Comparing the performance of the three Experiments using RIM-ONE (V2) database.

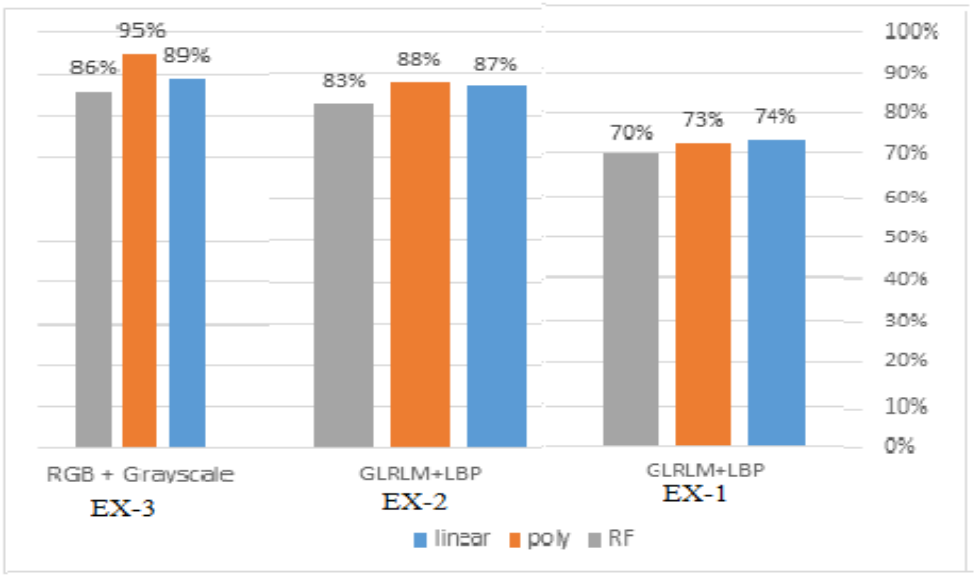

Figure 5.18: Comparing the performance of the three Experiments using RIM-ONE (V3) database.

CHAPTER SIX

Conclusion

6.1 Conclusion

The glaucoma diagnosis using computational approaches aimed to support specialists in disease identification and to prevent the glaucoma development. This work proposed an automated glaucoma diagnosis system by extracting texture features using LBP and GLRLM descriptors from fundus images and applied linear, polynomial SVM and RF classifiers to get classification models of glaucoma detection, three different experiments were applied.

In first experiment, the system was investigated without preprocessing method that led to obtain low results, where in the second experiment, the powerful of preprocessing phase was observed, and how the results improved rapidly compared to first experiment. This work concluded that preprocessing the data had critical role to improve the pattern recognition and classification performance and the performance was not effected with segmentation error due to extract non-morphological features.

In addition, used separated channels of image provided more information about the texture of the image and contributed to increase the performance.

In third experiment, the two extracted methods were combine in different manner of second experiment, where LBP method was adapted to generate binary representations of R-G-B image channels and grayscale of an image, GLRLM extracted the features from LBP represented images. The results showed that the SVM classifier was achieved a promising success rate of 98%, 91%, and 97% for RIM-ONE V1, V2, and V3 database respectively, comparing the linear SVM results with RF classifier and the studies in related literature results that used the same database and classifier. The proposed method achieved the highest results, where it had low cost and used limited resources.

The first contribution in our research was using all GLRLM features in automated glaucoma detection and obtaining promising results, the second contribution was the conjunction between GLRLM and LBP methods, where GLRLM was applied on binary representation on LBP.

When the ophthalmologists screened the misclassified images of our system, their results were about 50% of images classified correctly, where the other images stated as misdiagnosed or not clear and need to additional measurements that observed the worthiness of our methodology.

The research concluded that using image channels with grayscale provided more information of images, while combining different feature extraction methods led to increase the results. Extracted GLRLM features from binary LBP representations to obtain characteristics of image pattern improved the performance more than traditional histogram features that used in the second experiment and in the literature reviews (Claro et al., 2019) (Krishnamoorthi & Chinnababu, 2019) (Chaudhary & Pachori, 2021) and (de Sousa et al., 2017). Furthermore, preprocessing and dimensionality reduction methods had a critical role to improve performance by achieving discriminant features vector.

6.2 Limitation of Research

It was difficult to construct model deal with all problem aspects, the following points indicate the limitations of this work:

1) Glaucoma disease had different types and degrees of severity; this work just identified glaucoma and healthy eye.
2) Due to extract non-morphological features, the segmentation of database images was not required.
3) The small number of images in fundus images datasets or in other types of retinal images datasets that were used in eye diseases area could limit the results.
4) Different types of retinal images used to glaucoma diagnosis, because of low cost and popularity, fundus images were used in our work.
5) Lack early glaucoma data leaded us to difficulty to glaucoma diagnosis in early stages.

6.3 Future Work

The extracted features of the average of gray level matrices described the global view of the texture information. Future work extracted features from run length matrix each direction alone that most discriminative features were kept and removed correlated features that reflected the characteristics of an image.

For future work, the researcher believed:

1) The results could improve by using additional feature extraction methods.
2) Testing our method with other public glaucoma databases.
3) Adapte our methodology on other eye diseases, such as cataracts.
4) Detect the progresses of the glaucoma in early stages.

References

Acharya, U. R., Ng, E., Eugene, L. W. J., Noronha, K. P., Min, L. C., Nayak, K. P., & Bhandary, S. V. (2015). Decision support system for the glaucoma using Gabor transformation. *Biomedical Signal Processing and Control, 15*, 18-26.

Agarwal, A., Gulia, S., Chaudhary, S., Dutta, M. K., Burget, R., & Riha, K. (2015). *Automatic glaucoma detection using adaptive threshold based technique in fundus image.* Paper presented at the 2015 38th International Conference on Telecommunications and Signal Processing (TSP).

Ahn, J. M., Kim, S., Ahn, K.-S., Cho, S.-H., Lee, K. B., & Kim, U. S. (2018). A deep learning model for the detection of both advanced and early glaucoma using fundus photography. *PloS one, 13*(11), e0207982.

Ahonen, T., Hadid, A., & Pietikäinen, M. (2004). *Face recognition with local binary patterns.* Paper presented at the European conference on computer vision.

Al-Bander, B., Al-Nuaimy, W., Al-Taee, M. A., & Zheng, Y. (2017). *Automated glaucoma diagnosis using deep learning approach.* Paper presented at the 2017 14th International Multi-Conference on Systems, Signals & Devices (SSD).

Al Ghamdi, M., Li, M., Abdel-Mottaleb, M., & Abou Shousha, M. (2019). *Semi-supervised transfer learning for convolutional neural networks for glaucoma detection.* Paper presented at the ICASSP 2019-2019 IEEE International Conference on Acoustics, Speech and Signal Processing (ICASSP).

Almazroa, A., Alodhayb, S., Osman, E., Ramadan, E., Hummadi, M., Dlaim, M., . . . Lakshminarayanan, V. (2018). *Retinal fundus images for glaucoma analysis: the RIGA dataset.* Paper presented at the Medical Imaging 2018: Imaging Informatics for Healthcare, Research, and Applications.

An, G., Omodaka, K., Hashimoto, K., Tsuda, S., Shiga, Y., Takada, N., . . . Nakazawa, T. (2019). Glaucoma diagnosis with machine learning based on optical coherence tomography and color fundus images. *Journal of healthcare engineering, 2019*.

An, G., Omodaka, K., Tsuda, S., Shiga, Y., Takada, N., Kikawa, T., . . . Akiba, M. (2018). Comparison of machine-learning classification models for glaucoma management. *Journal of healthcare engineering, 2018*.

Anusorn, C. B., Kongprawechnon, W., Kondo, T., Sintuwong, S., & Tungpimolrut, K. (2013). Image processing techniques for glaucoma detection using the cup-to-disc ratio. *Science & Technology Asia*, 22-34.

Ayub, J., Ahmad, J., Muhammad, J., Aziz, L., Ayub, S., Akram, U., & Basit, I. (2016). *Glaucoma detection through optic disc and cup segmentation using K-mean clustering.* Paper presented at the 2016 international conference on computing, electronic and electrical engineering (ICE Cube).

Bajwa, M. N., Malik, M. I., Siddiqui, S. A., Dengel, A., Shafait, F., Neumeier, W., & Ahmed, S. (2019). Two-stage framework for optic disc localization and glaucoma classification in retinal fundus images using deep learning. *BMC medical informatics and decision making, 19*(1), 1-16.

Bisneto, T. R. V., de Carvalho Filho, A. O., & Magalhães, D. M. V. (2020). Generative adversarial network and texture features applied to automatic glaucoma detection. *Applied Soft Computing, 90*, 106165.

Bowd, C., & Goldbaum, M. H. (2008). Machine learning classifiers in glaucoma. *Optometry and Vision Science, 85*(6), 396-405.

Breiman, L. (2001). Random forests. *Machine learning, 45*(1), 5-32.

Burlina, P. M., Joshi, N., Pekala, M., Pacheco, K. D., Freund, D. E., & Bressler, N. M. (2017). Automated grading of age-related macular degeneration from color fundus images using deep convolutional neural networks. *JAMA ophthalmology, 135*(11), 1170-1176.

Carmona, E. J., Rincón, M., García-Feijoó, J., & Martínez-de-la-Casa, J. M. (2008). Identification of the optic nerve head with genetic algorithms. *Artificial intelligence in medicine, 43*(3), 243-259.

Cerentini, A., Welfer, D., d'Ornellas, M. C., Haygert, C. P., & Dotto, G. (2018). Automatic identification of glaucoma using deep learning methods. *Proc. 16th World Congr. Med. Health Informat. Precision Healthcare Through Informat.(MEDINFO), 245*, 318.

Chaudhary, P. K., & Pachori, R. B. (2021). Automatic diagnosis of glaucoma using two-dimensional Fourier-Bessel series expansion based empirical wavelet transform. *Biomedical Signal Processing and Control, 64*. doi:10.1016/j.bspc.2020.102237

Chen, X., Xu, Y., Wong, D. W. K., Wong, T. Y., & Liu, J. (2015). *Glaucoma detection based on deep convolutional neural network.* Paper presented at the 2015 37th annual international conference of the IEEE engineering in medicine and biology society (EMBC).

Chen, X., Xu, Y., Yan, S., Wong, D. W. K., Wong, T. Y., & Liu, J. (2015). *Automatic feature learning for glaucoma detection based on deep learning.* Paper presented at the International conference on medical image computing and computer-assisted intervention.

Chrástek, R., Wolf, M., Donath, K., Niemann, H., Paulus, D., Hothorn, T., . . . Michelson, G. (2005). Automated segmentation of the optic nerve head for diagnosis of glaucoma. *Medical image analysis, 9*(4), 297-314.

Chu, A., Sehgal, C., & Greenleaf, J. (1991). Use of gray value distribution of run lengths for texture analysis. *Pattern Recognition Letters, 12*(1991), 65.

Chu, A., Sehgal, C. M., & Greenleaf, J. F. (1990). Use of gray value distribution of run lengths for texture analysis. *Pattern Recognition Letters, 11*(6), 415-419.

Claro, M., Veras, R., Santana, A., Araújo, F., Silva, R., Almeida, J., & Leite, D. (2019). An hybrid feature space from texture information and transfer learning for glaucoma classification. *Journal of Visual Communication and Image Representation, 64*. doi:10.1016/j.jvcir.2019.102597

Costa, P., Galdran, A., Meyer, M. I., Niemeijer, M., Abràmoff, M., Mendonça, A. M., & Campilho, A. (2017). End-to-end adversarial retinal image synthesis. *IEEE transactions on medical imaging, 37*(3), 781-791.

Dasarathy, B. V., & Holder, E. B. (1991). Image characterizations based on joint gray level—run length distributions. *Pattern Recognition Letters, 12*(8), 497-502.

de Carvalho Junior, A. S. V., Carvalho, E. D., de Carvalho Filho, A. O., de Sousa, A. D., Silva, A. C., & Gattass, M. (2018). Automatic methods for diagnosis of glaucoma using texture descriptors based on phylogenetic diversity. *Computers & Electrical Engineering, 71*, 102-114.

de Sales Carvalho, N. R., Rodrigues, M. d. C. L. C., de Carvalho Filho, A. O., & Mathew, M. J. (2021). Automatic method for glaucoma diagnosis using a three-dimensional convoluted neural network. *Neurocomputing, 438*, 72-83.

de Sousa, J. A., de Paiva, A. C., Sousa de Almeida, J. D., Silva, A. C., Junior, G. B., & Gattass, M. (2017). Texture based on geostatistic for glaucoma diagnosis from fundus eye image. *Multimedia Tools and Applications, 76*(18), 19173-19190.

Devasia, T., Jacob, K. P., & Thomas, T. (2019). Automatic early stage glaucoma detection using cascade correlation neural network. In *Smart Intelligent Computing and Applications* (pp. 659-669): Springer.

Dey, A., & Bandyopadhyay, S. K. (2016). Automated glaucoma detection using support vector machine classification method. *British Journal of Medicine and Medical Research, 11*(12), 1.

Dey, A., & Dey, K. N. (2018). Automated glaucoma detection from fundus images of eye using statistical feature extraction methods and support vector machine classification. In *Industry Interactive Innovations in Science, Engineering and Technology* (pp. 511-521): Springer.

Diaz-Pinto, A., Colomer, A., Naranjo, V., Morales, S., Xu, Y., & Frangi, A. F. (2019). Retinal image synthesis and semi-supervised learning for glaucoma assessment. *IEEE transactions on medical imaging, 38*(9), 2211-2218.

dos Santos Ferreira, M. V., de Carvalho Filho, A. O., de Sousa, A. D., Silva, A. C., & Gattass, M. (2018). Convolutional neural network and texture descriptor-based automatic detection and diagnosis of glaucoma. *Expert Systems with Applications, 110*, 250-263.

Dua, S., Acharya, U. R., Chowriappa, P., & Sree, S. V. (2011). Wavelet-based energy features for glaucomatous image classification. *Ieee transactions on information technology in biomedicine, 16*(1), 80-87.

Elseid, A. A. G., & Hamza, A. O. (2018). Glaucoma detection based on shape features and SMOTE algorithm. *CiiT International Journal of Digital Image Processing, 10*(10).

Fu, H., Xu, Y., Lin, S., Kee Wong, D. W., & Liu, J. (2016). *Deepvessel: Retinal vessel segmentation via deep learning and conditional random field.* Paper presented at the International conference on medical image computing and computer-assisted intervention.

Fumero, F., Alayón, S., Sanchez, J. L., Sigut, J., & Gonzalez-Hernandez, M. (2011). *RIM-ONE: An open retinal image database for optic nerve evaluation.* Paper presented at the 2011 24th international symposium on computer-based medical systems (CBMS).

Galloway, M. M. (1975). Texture analysis using gray level run lengths. *Computer graphics and image processing, 4*(2), 172-179.

Ghassabeh, Y. A., Rudzicz, F., & Moghaddam, H. A. (2015). Fast incremental LDA feature extraction. *Pattern Recognition, 48*(6), 1999-2012.

Gholami, R., & Fakhari, N. (2017). Support Vector Machine: Principles, Parameters, and Applications. In *Handbook of Neural Computation* (pp. 515-535).

Goldbaum, M. H., Sample, P. A., White, H., Colt, B., Raphaelian, P., Fechtner, R. D., & Weinreb, R. N. (1994). Interpretation of automated perimetry for glaucoma by neural network. *Investigative ophthalmology & visual science, 35*(9), 3362-3373.

Gómez-Valverde, J. J., Antón, A., Fatti, G., Liefers, B., Herranz, A., Santos, A., . . . Ledesma-Carbayo, M. J. (2019). Automatic glaucoma classification using color fundus images based on convolutional neural networks and transfer learning. *Biomedical optics express, 10*(2), 892-913.

Guo, Z., Zhang, L., & Zhang, D. (2010). A completed modeling of local binary pattern operator for texture classification. *IEEE transactions on image processing, 19*(6), 1657-1663.

Haleem, M. S., Han, L., Van Hemert, J., & Li, B. (2013). Automatic extraction of retinal features from colour retinal images for glaucoma diagnosis: a review. *Computerized medical imaging and graphics, 37*(7-8), 581-596.

Holm, S., Russell, G., Nourrit, V., & McLoughlin, N. (2017). DR HAGIS—a fundus image database for the automatic extraction of retinal surface vessels from diabetic patients. *Journal of Medical Imaging, 4*(1), 014503.

Huang, M.-L., Chen, H.-Y., & Huang, J.-J. (2007). Glaucoma detection using adaptive neuro-fuzzy inference system. *Expert Systems with Applications, 32*(2), 458-468.

Huang, X., Li, S. Z., & Wang, Y. (2004). *Shape localization based on statistical method using extended local binary pattern.* Paper presented at the Third International Conference on Image and Graphics (ICIG'04).

Issac, A., Sarathi, M. P., & Dutta, M. K. (2015). An adaptive threshold based image processing technique for improved glaucoma detection and classification. *Computer methods and programs in biomedicine, 122*(2), 229-244.

Jackson, A., & Radhakrishnan, S. (2014). Understanding and living with Glaucoma. *Glaucoma Research Foundation*.

Jiang, Y., Tan, N., & Peng, T. (2019). Optic disc and cup segmentation based on deep convolutional generative adversarial networks. *IEEE Access, 7*, 64483-64493.

Kadlček, F., & Fucik, O. (2012). *Evolutionary design of local binary pattern feature shapes for object detection.* Paper presented at the 2012 NASA/ESA Conference on Adaptive Hardware and Systems (AHS).

Kavya, N., & Padmaja, K. (2017). *Glaucoma detection using texture features extraction.* Paper presented at the 2017 51st Asilomar Conference on Signals, Systems, and Computers.

Khan, S. I., Choubey, S. B., Choubey, A., Bhatt, A., Naishadhkumar, P. V., & Basha, M. M. (2021). Automated glaucoma detection from fundus images using

wavelet-based denoising and machine learning. *Concurrent Engineering*. doi:10.1177/1063293x211026620

Kim, S. J., Cho, K. J., & Oh, S. (2017). Development of machine learning models for diagnosis of glaucoma. *PloS one, 12*(5), e0177726.

Krishnamoorthi, N., & Chinnababu, V. K. (2019). Hybrid feature vector based detection of Glaucoma. *Multimedia Tools and Applications, 78*(24), 34247-34276.

Krishnan, M. M. R., & Faust, O. (2013). Automated glaucoma detection using hybrid feature extraction in retinal fundus images. *Journal of Mechanics in Medicine and Biology, 13*(01), 1350011.

Kucur, Ş. S., Hollo, G., & Sznitman, R. (2018). A deep learning approach to automatic detection of early glaucoma from visual fields. *PloS one, 13*(11), e0206081.

Kumar, J., Seelamantula, C. S., Kamath, Y. S., & Jampala, R. (2019). Rim-to-disc ratio outperforms cup-to-disc ratio for glaucoma prescreening. *Scientific reports, 9*(1), 1-9.

Madhusudhan, M., Malay, N., Nirmala, S., & Samerendra, D. (2011). *Image processing techniques for glaucoma detection.* Paper presented at the International conference on advances in computing and communications.

Maheshwari, S., Pachori, R. B., & Acharya, U. R. (2016). Automated diagnosis of glaucoma using empirical wavelet transform and correntropy features extracted from fundus images. *IEEE journal of biomedical and health informatics, 21*(3), 803-813.

Mansour, R. F. (2017). Evolutionary computing enriched computer-aided diagnosis system for diabetic retinopathy: a survey. *IEEE reviews in biomedical engineering, 10*, 334-349.

Mansour, R. F., & Al-Marghilnai, A. (2021). Glaucoma detection using novel perceptron based convolutional multi-layer neural network classification. *Multidimensional Systems and Signal Processing, 32*(4), 1217-1235. doi:10.1007/s11045-021-00781-0

Martínez-Ramón, M., & Christodoulou, C. (2005). Support vector machines for antenna array processing and electromagnetics. *Synthesis Lectures on Computational Electromagnetics, 1*(1), 1-120.

Mayro, E. L., Wang, M., Elze, T., & Pasquale, L. R. (2020). The impact of artificial intelligence in the diagnosis and management of glaucoma. *Eye, 34*(1), 1-11.

Medeiros, F. A., Jammal, A. A., & Thompson, A. C. (2019). From machine to machine: an OCT-trained deep learning algorithm for objective quantification of glaucomatous damage in fundus photographs. *Ophthalmology, 126*(4), 513-521.

Meier, J., Bock, R., Michelson, G., Nyul, L. G., & Hornegger, J. (2007). *Effects of Preprocessing Eye Fundus Images on Appearance Based Glaucoma Classification.* Paper presented at the Computer Analysis of Images and Patterns: 12th International Conference, CAIP 2007, Vienna, Austria, August 27-29, 2007, Proceedings.

Nayak, J., Acharya U, R., Bhat, P. S., Shetty, N., & Lim, T.-C. (2009). Automated diagnosis of glaucoma using digital fundus images. *Journal of medical systems, 33*(5), 337-346.

Nyúl, L. G. (2009). *Retinal image analysis for automated glaucoma risk evaluation.* Paper presented at the MIPPR 2009: Medical Imaging, Parallel Processing of Images, and Optimization Techniques.

Odstrcilik, J., Kolar, R., Budai, A., Hornegger, J., Jan, J., Gazarek, J., . . . Angelopoulou, E. (2013). Retinal vessel segmentation by improved matched filtering: evaluation on a new high-resolution fundus image database. *IET Image Processing, 7*(4), 373-383.

Orlando, J. I., Fu, H., Breda, J. B., van Keer, K., Bathula, D. R., Diaz-Pinto, A., . . . Lee, J. (2020). Refuge challenge: A unified framework for evaluating automated methods for glaucoma assessment from fundus photographs. *Medical image analysis, 59*, 101570.

Parashar, D., & Agrawal, D. (2020). *Automated classification of glaucoma using retinal fundus images.* Paper presented at the 2020 First IEEE International Conference on Measurement, Instrumentation, Control and Automation (ICMICA).

Parashar, D., & Agrawal, D. (2021). *Improved classification of glaucoma in retinal fundus images using 2D-DWT.* Paper presented at the 2021 International Conference on Advances in Electrical, Computing, Communication and Sustainable Technologies (ICAECT).

Parashar, D., & Agrawal, D. (2021). *Texture-based feature extraction from fundus images for glaucoma diagnosis.* Paper presented at the 2021 Sixth International Conference on Wireless Communications, Signal Processing and Networking (WiSPNET).

Quigley, H. A., & Broman, A. T. (2006). The number of people with glaucoma worldwide in 2010 and 2020. *British journal of ophthalmology, 90*(3), 262-267.

Raghavendra, U., Fujita, H., Bhandary, S. V., Gudigar, A., Tan, J. H., & Acharya, U. R. (2018). Deep convolution neural network for accurate diagnosis of glaucoma using digital fundus images. *Information Sciences, 441*, 41-49.

Rajyaguru, V., Vithalani, C., & Thanki, R. (2020). A literature review: various learning techniques and its applications for eye disease identification using retinal images. *International Journal of Information Technology*, 1-12.

Saba, T., Bokhari, S. T. F., Sharif, M., Yasmin, M., & Raza, M. (2018). Fundus image classification methods for the detection of glaucoma: A review. *Microscopy research and technique, 81*(10), 1105-1121.

Sahu, S., Singh, H. V., Kumar, B., Singh, A. K., & Kumar, P. (2019). Image processing based automated glaucoma detection techniques and role of de-noising: a technical survey. In *Handbook of Multimedia Information Security: Techniques and Applications* (pp. 359-375): Springer.

Salam, A. A., Khalil, T., Akram, M. U., Jameel, A., & Basit, I. (2016). Automated detection of glaucoma using structural and non structural features. *Springerplus, 5*(1), 1-21.

Şendur, L., & Selesnick, I. W. (2002). *A bivariate shrinkage function for wavelet-based denoising.* Paper presented at the 2002 IEEE International Conference on Acoustics, Speech, and Signal Processing.

Septiarini, A., & Harjoko, A. (2015). AUTOMATIC GLAUCOMA DETECTION BASED ON THE TYPE OF FEATURES USED: A REVIEW. *Journal of Theoretical & Applied Information Technology, 72*(3).

Serener, A., & Serte, S. (2019). *Transfer learning for early and advanced glaucoma detection with convolutional neural networks.* Paper presented at the 2019 Medical technologies congress (TIPTEKNO).

Sevastopolsky, A. (2017). Optic disc and cup segmentation methods for glaucoma detection with modification of U-Net convolutional neural network. *Pattern Recognition and Image Analysis, 27*(3), 618-624.

Sevastopolsky, A., Drapak, S., Kiselev, K., Snyder, B. M., Keenan, J. D., & Georgievskaya, A. (2019). *Stack-u-net: refinement network for improved optic disc and cup image segmentation.* Paper presented at the Medical Imaging 2019: Image Processing.

Shinde, R. (2021). Glaucoma detection in retinal fundus images using U-Net and supervised machine learning algorithms. *Intelligence-Based Medicine, 5*. doi:10.1016/j.ibmed.2021.100038

Simón, M. A., Alonso, L., & Antón, A. (2005). A hybrid visual field classifier to support early glaucoma diagnosis. *Inteligencia Artificial. Revista Iberoamericana de Inteligencia Artificial, 9*(26), 9-17.

Singh, L., & Garg, H. (2019). A Novel Deep Learning Approach for Detection of Glaucoma. *Jour of Adv Research in Dynamical& Control Systems, 11*(04-Special Issue), 2543-2554.

Sivaswamy, J., Krishnadas, S., Joshi, G. D., Jain, M., & Tabish, A. U. S. (2014). *Drishti-gs: Retinal image dataset for optic nerve head (onh) segmentation.* Paper presented at the 2014 IEEE 11th international symposium on biomedical imaging (ISBI).

Soman, A., & Mathew, D. (2016). Glaucoma detection and segmentation using retinal images. *International Journal of Science, Engineering and Technology Research, 5*(5), 1346-1349.

Son, J., Park, S. J., & Jung, K.-H. (2019). Towards accurate segmentation of retinal vessels and the optic disc in fundoscopic images with generative adversarial networks. *Journal of digital imaging, 32*(3), 499-512.

Srinivasan, C., Dubey, S., & Ganeshbabu, T. (2016). Complex texture features for glaucomatous image classification system using fundus images. *International Journal of Engineering Research & Science, 2*(12), 106-113.

Suh, M. H., Kim, S. K., Park, K. H., Kim, D. M., Kim, S. H., & Kim, H. C. (2013). Combination of optic disc rim area and retinal nerve fiber layer thickness for early glaucoma detection by using spectral domain OCT. *Graefe's Archive for Clinical and Experimental Ophthalmology, 251*(11), 2617-2625.

Suruliandi, A., Meena, K., & Rose, R. R. (2012). Local binary pattern and its derivatives for face recognition. *IET computer vision, 6*(5), 480-488.

Thakur, N., & Juneja, M. (2020). Classification of glaucoma using hybrid features with machine learning approaches. *Biomedical Signal Processing and Control, 62*. doi:10.1016/j.bspc.2020.102137

Tham, Y.-C., Li, X., Wong, T. Y., Quigley, H. A., Aung, T., & Cheng, C.-Y. (2014). Global prevalence of glaucoma and projections of glaucoma burden through 2040: a systematic review and meta-analysis. *Ophthalmology, 121*(11), 2081-2090.

Toshev, A. P., Lamparter, J., Pfeiffer, N., & Hoffmann, E. M. (2017). Bruch's membrane opening-minimum rim width assessment with spectral-domain optical coherence tomography performs better than confocal scanning laser ophthalmoscopy in discriminating early glaucoma patients from control subjects. *Journal of Glaucoma, 26*(1), 27-33.

Van Griethuysen, J. J., Fedorov, A., Parmar, C., Hosny, A., Aucoin, N., Narayan, V., . . . Aerts, H. J. (2017). Computational radiomics system to decode the radiographic phenotype. *Cancer research, 77*(21), e104-e107.

Wang, L. (2005). *Support vector machines: theory and applications* (Vol. 177): Springer Science & Business Media.

Weinreb, R. N., Aung, T., & Medeiros, F. A. (2014). The pathophysiology and treatment of glaucoma: a review. *Jama, 311*(18), 1901-1911.

Wu, Y., Szymanska, M., Hu, Y., Fazal,M. I., Jiang, N., Yetisen, A. K., Cordeiro,M. F.(2022). Measures of disease activity in glaucoma. *Biosensors and Bioelectronics,*196. doi:10.1016/j.bios.2021.113700

Xanthopoulos, P., Pardalos, P. M., & Trafalis, T. B. (2012). *Robust data mining*: Springer Science & Business Media.

Xu, X., Zhang, L., Li, J., Guan, Y., & Zhang, L. (2019). A hybrid global-local representation CNN model for automatic cataract grading. *IEEE journal of biomedical and health informatics, 24*(2), 556-567.

Yousefi, S., Elze, T., Pasquale, L. R., & Boland, M. (2018). *Glaucoma monitoring using manifold learning and unsupervised clustering.* Paper presented at the 2018 International Conference on Image and Vision Computing New Zealand (IVCNZ).

Yu, W., Ma, Y., Zheng, L., & Liu, K. (2016). *Research of improved adaptive median filter algorithm.* Paper presented at the Proceedings of the 2015 international conference on Electrical and Information Technologies for Rail Transportation.

Zhang, Z., Yin, F. S., Liu, J., Wong, W. K., Tan, N. M., Lee, B. H., . . . Wong, T. Y. (2010). *Origa-light: An online retinal fundus image database for glaucoma analysis and research.* Paper presented at the 2010 Annual international conference of the IEEE engineering in medicine and biology.

Zhao, R., Chen, X., Chen, Z., & Li, S. (2022). Diagnosing glaucoma on imbalanced data with self-ensemble dual-curriculum learning. *Medical image analysis, 75*, 102295.

Zheng, C., Johnson, T. V., Garg, A., & Boland, M. V. (2019). Artificial intelligence in glaucoma. *Current opinion in ophthalmology, 30*(2), 97-103.

اكتشاف زرق العين آلياً باستخدام مزيج من طرق استخراج الميزات

قدم من قبل:

زكية أحمد علي

تحت إشراف:

د. أحمد الاوجلي

مشرف مساعد:

د. محمد عبدالله

الملخص

تستخدم تقنيات التعلم الآلي بشكل متزايد في تحليل الصور الطبية للتعرف على الميزات واتخاذ القرار وبالتالي توضح التقدم في مجال الرعاية الطبية. يساهم التحليل الآلي للصور الطبية في زيادة أداء التصنيف. زيادة عدد مرضى زرق العين في بلادنا حفزنا على إنشاء نظام آلي لاكتشاف المرض. زرق العين هو مرض مزمن وتنكسي يسبب تلفً دائم في الجهاز العصبي للعين ويؤدي إلى العمى. يهدف هذا البحث إلى تقديم نهج آلي للكشف عن زرق العين بتحديد السمات غير الشكلية باستخدام مزيج من طرق استخراج الميزات. تم تقسيم المنهجية المقترحة إلى: الحصول على الصور من خلال قاعدة البيانات RIM-ONEs، تم تطبيق 2D-Discrete Wavelet Transform على صور قواعد البيانات لإزالة الضوضاء. ثم تمثيل الصور المقسمة باستخدام Local Binary Pattern واستخدمت Grey Level Run-Length Matrix لوصف تركيب الانماط. أخيراً تم تطبيق اثنين من المصنفات لتعليم النماذج باستخدام الميزات المستخرجة, المنهجية المقترحة قيمت بواسطة الحساسية والخصوصية ودقة النماذج والنتائج كانت واعدة وأكثر دقة مقارنة بالدراسات السابقة.

جامعة بنغازي
كلية تقنية المعلومات
قسم علوم الحاسوب

اكتشاف زرق العين أليا باستخدام مزيج من طرق استخراج الميزات

قدمت من قبل:
زكية أحمد علي بالقاسم

تحت اشراف
احمد الاوجلي
أستاذ مشارك
مشرف مساعد
محمد عبدالله
أستاذ مساعد

قدمت هذه الرسالة استكمالا لمتطلبات الحصول على درجة الماجستير في علوم الحاسوب

بتاريخ 25\1\ 2023 م الموافق 2\رجب\1444ه